NSTX Upgrade

OH Coaxial Cable and Embedded Leads

NSTXU-CALC-133-07-00

10 October 2011

Prepared By:

Michael Mardenfeld

Digitally signed by Michael Mardenfeld
DN: cn=Michael Mardenfeld, o=PPPL, ou=Mechanical Eng Design, email=mmarden@pppl.gov, c=US
Date: 2011.10.11 14:05:37 -04'00'

Michael Mardenfeld, PPPL Mechanical Engineering

Reviewed By:

Ali Zolfaghari

Digitally signed by Ali Zolfaghari
DN: cn=Ali Zolfaghari, o=PPPL, ou=Engineering, email=azolfagh@pppl.gov, c=US
Date: 2011.10.11 14:25:33 -04'00'

Ali Zolfaghari, PPPL Mechanical Engineering

Reviewed By:

James H. Chrzanowski

Digitally signed by James H. Chrzanowski
DN: cn=James H. Chrzanowski, o=PPPL, ou=Mech Engineering, email=jchrzano@pppl.gov, c=US
Date: 2011.10.11 15:06:06 -04'00'

Jim Chrzanowski, Cognizant Engineer

PPPL Calculation Form

Calculation # **NSTXU-CALC-133-07-00** Revision # **00** WP #, if any **1305**

Purpose of Calculation: (Define why the calculation is being performed.)

To qualify those components providing an electrical path between the bus bars and the main body of the OH coil, i.e., the coaxial cable, electrical connectors, and embedded coil leads.

References (List any source of design information including computer program titles and revision levels.)

NSTXU-CALC-133-09-00 Rev 0 **OH Conductor Fatigue & Fracture Mechanics**
NSTXU-CALC-133-08-00 Rev 0 **OH Stress Analysis**
NSTXU-ALC-55-01-00 Rev 0 **Bus Bar Analysis**
CTD Final Test Report, 4/8/2011, PPPL Purchase Order PE010637-W **Short Beam Shear Testing,**
Calculated Poloidal Magnetics Quantities for the May 4, 2010 **Memo, R. Woolley, 17 December 2010**
Design of the NSTX CS Upgrade

Matlab Script, documented in NSTXU-CALC-13-01-00 Rev 0
NSTX Upgrade General Requirements Document Rev 3

Assumptions (Identify all assumptions made as part of this calculation.):

See Section 3.0.

.

Calculation (Calculation is either documented here or attached):

See Attached.

Conclusion (Specify whether or not the purpose of the calculation was accomplished.)

Pending minor design changes, NSTX-U Coaxial Cable and Embedded Leads meet all design criteria.

Cognizant Engineer's printed name, signature, and date

James H. Chrzanowski Digitally signed by James H. Chrzanowski
DN: cn=James H. Chrzanowski, o=PPPL, ou=Mech Engineering, email=jchrzano@pppl.gov, c=US
Date: 2011.10.11 15:06:18 -04'00'

I have reviewed this calculation and, to my professional satisfaction, it is properly performed and correct.

Checker's printed name, signature, and date

Ali Zolfaghari Digitally signed by Ali Zolfaghari
DN: cn=Ali Zolfaghari, o=PPPL, ou=Engineering, email=azolfagh@pppl.gov, c=US
Date: 2011.10.11 14:26:16 -04'00'

Minimum Requirements for Checking of Calculations

1. Assure that inputs were correctly selected and incorporated into the design.

2. Calculation considers, as appropriate:

   - Performance Requirements (capacity, rating, system output)
   - Design Conditions (pressure, temperature, voltage, etc.)
   - Load Conditions (seismic, wind, thermal, dynamic)
   - Environmental Conditions (radiation zone, hazardous material, etc.)
   - Material Requirements
   - Structural Requirements (foundations, pipe supports, etc.)
   - Hydraulic Requirements (NPSH, pressure drops, etc.)
   - Chemistry Requirements
   - Electrical Requirements (power source, volts, raceway, and insulation)
   - Equipment Reliability (FMEA)
   - Failure Effects on Surrounding Equipment
   - Tolerance Buildup

3. Assumptions necessary to perform the design activity are adequately described and reasonable.

4. An appropriate calculation method was used.

5. The results are reasonable compared to the inputs.

NOTE: IT IS THE RESPONSIBILITY OF THE CHECKER TO USE METHODS THAT WILL SUBSTANTIATE TO HIS/HER PROFESSIONAL SATISFACTION THAT THE CALCULATION IS CORRECT.

BY SIGNING CALCULATION, CHECKER ACKNOWLEDGES THAT THE CALCULATION HAS BEEN APPROPRIATELY CHECKED AND THAT THE APPLICABLE ITEMS LISTED ABOVE HAVE BEEN INCLUDED AS PART OF THE CHECK.

I have reviewed this calculation and, to my professional satisfaction, it is properly performed and correct.

Checker's printed name, signature, and date

Executive Summary

The purpose of this calculation is to qualify those components of the NSTX Upgrade which either provide an electrical path between the OH bus bar, and the body of the OH coil itself, or are ancillary structural members directly adjacent to this electrical path. Key Conclusions as are follows:

1. **The steel clamp connecting the bus bar to the skirt is not stiff enough as is, and will be need to be reinforced**. The stresses calculated with clamp as is are an order of magnitude too high. This is in agreement with the bus bar analysis (NSTXU-Calc-55-01). For this calculation, the clamp is assumed to be "infinitely rigid", by applying a fixed boundary at the bus bar/clamp interface. An appropriate clamp, which directs all bus bar reaction forces away from the coaxial cable, needs to be designed and qualified as acceptable for the bus bar.

2. **In the current design, there is a short section of conductor, where the leads "break out" of the G10 annulus and are brazed onto the lead flags, which is subject to particularly high thermal stress.** The lead flags should be slightly modified to include a fillet near this braze joint, and the conductor should be encapsulated with a structural filler material (i.e. glass reinforced room temperature curing epoxy). With these modifications, the peak tensile principle stress is reduced to ~ 80 Mpa, and the peak Stress Intensity is reduced to ~ 190 Mpa, which are within allowable.

3. **Per results of NSTXU-Calc-55-01, the OH bus bars will be modified to include active cooling.** The inlet temperature for this coolant should be the same as the inlet temperature for the OH coolant water, nominally 12 C. Furthermore, the coolant inlet should be near the coaxial cable end of the bus bar, and the outlet should be at the power supply side of the bus bar, such that the water is flowing away from the machine. In this way, thermal gradients across the coaxial cable are minimized, and there is sufficient conduction from the coaxial cable to the actively cooled bus bar and lead flags that there will be no ratcheting, and the coax will cool down completely between shots.

4. **Provided adequate structural support redirects bus bar reaction forces away from the coax per item one, Lorentz forces are not high enough to be of any significance. These components are overwhelmingly driven by thermal effects.** During normal operation, local peak stress intensity and tensile principal stresses from electromagnetic forces only are ~ 25 Mpa and 7 Mpa respectively, with membrane stresses << 10 Mpa. Although only electromagnetic equilibria were considered, these values are so low that even if they were doubled during transients or disruptions, the stresses would still be acceptable.

5. **The delaminating shearing stresses on the lead are of order 60 Mpa, above the fatigue allowable**. In the region, local delamination is expected, and acceptable, because testing has shown that it occurs in a predictably benign fashion, and the G10 Annulus will provide sufficient structural stability and dielectric strength.

6. **The shearing stress between the G10 Annulus and the lower most turns of the OH coil is of order 20 Mpa.** This is caused by the interaction between radial thermal expansion of the OH coil, and the fixity of the bottom of the cold G10 Annulus. The conductor within several layers of either the top or bottom of the OH coil should be sandblasted and primed to locally increase the shear strength. Locally these stresses are still above the 5x life fatigue requirement, after applying a 50% knockdown factor for interleaved Kapton. Progressive local delamination is likely, but judged acceptable.

Provided the recommended design changes are addressed, the analysis concludes that the thermal and mechanical response of OH coaxial and embedded leads are within acceptable ranges.

Table of Contents

1.0 Introduction

The purpose of this calculation is to qualify those components of the NSTX Upgrade which either provide an electrical path between the OH bus bar, and the body of the OH coil itself, or are ancillary structural members directly adjacent to this electrical path.

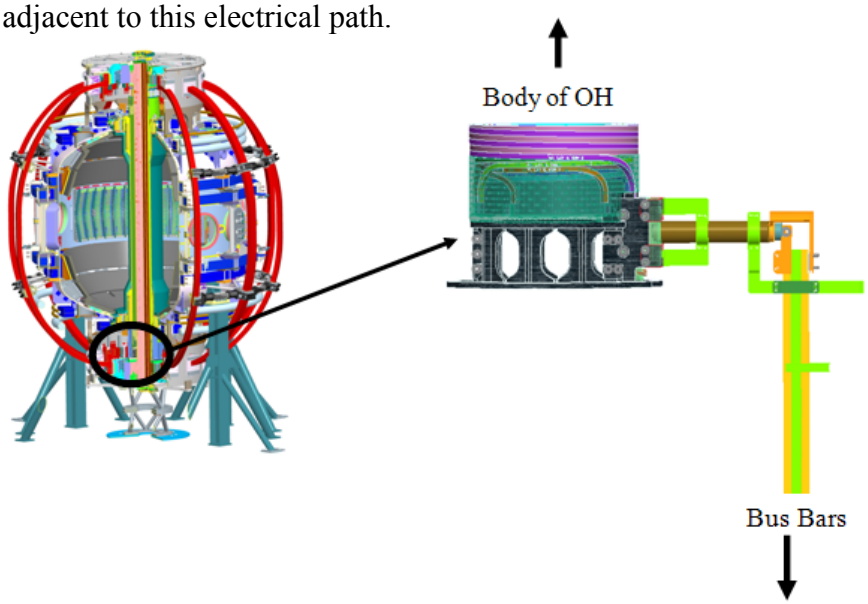

The main body of the OH coil, detailed in calculation NSTXU-Calc-133-08, is constructed from extruded copper conductors, which are wrapped with fiberglass cloth and Kapton insulation, wound into a solenoid, and vacuum pressure impregnated into a monolithic structure with an epoxy/cyanate ester insulation. The very bottom of this monolithic structure is an annular block of G10 ("G10 Annulus"), approximately 7 inches high, with the same cross section as the coil proper. This region encapsulates the electrical leads, water feeds, and provides a point for fixing the coil onto the steel support below. The electrical leads break out of this annulus, and are brazed to flat copper plates ("Lead Flags"), which are in turn brazed to the "coaxial cable". This entire region ("Coax Box") is also encapsulated in G10, which is hard shimmed, rather than impregnated. The coaxial cable provides a force balanced current path from the lead flags to the OH Bus bar, is detailed in calculation NSTXU-Calc-55-01. These components are exposed to currents of ~ 24 kAmps in magnetic fields of ≤ 3 Tesla, as well as thermal gradients induced by temperature excursions of up to ~ 85 C in ~ 8 seconds.

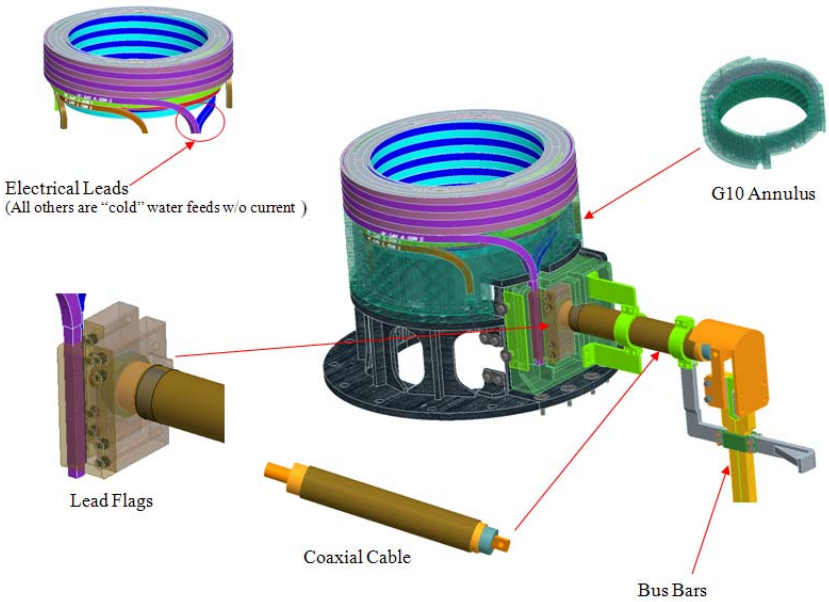

2.0 Material Properties and Design Criteria

Material properties used for this analysis are tabulated below.

Property	Units	Copper OFHC	G10/ Impregnated Insulation	Structural Filler ("Hysol")	Steel
Elastic Modulus	Pa	1.10E+11	2.00E+10	5.00E+09	2.00E+11
Poisson Ratio	unitless ratio	0.334	0.144	0.144	0.3
Density	kg / m^3	8300	1900	1900	7850
Resistivity	ohm m	1.96E-08	8.20E+13	8.20E+13	1.70E-07
Coefficient of Thermal Expansion	1 / K	1.8E-05	1.4E-05	1.4E-05	1.2E-05
Thermal Conductivity	W / (m K)	401	0.50	0.5	60.5
Specific Heat	J /(kg K)	385	2000	2000	434

All materials are assumed to be isotropic; this has been shown to be appropriate for G10 and vacuum impregnated, glass reinforced epoxy insulation by past experience. Since the resistivity of copper is strongly a function of temperature over the range 12 C to 100 C, but the electric analysis was NOT coupled and concurrently solved with the thermal analysis, the average value of the resistivity of copper was chosen.

Stress allowables for copper are taken from NSTXU-Calc-133-09, shown below. According to NSTX design criteria, an SN fatigue qualification (2X stress, 20X life) is not necessary, provided the fracture mechanics qualification of Max Principle Stress < 125 Mpa is met.

Criteria	Stress Level ant Type	Actual ref [1]
SN 2 on stress	112 MPa (Tresca)	142
SN 20 on life	180 (Tresca)	142
Fracture Mechanics with a flaw size less than .7mm 1.5 on KIc and 2 on Cycles	140 MPa (Max Principal or Hoop)	101
4 on cycles	125 MPa (Max Principal or Hoop)	101

This document also quotes a Sm (static primary membrane stress allowable) of 156 Mpa, and a bending + membrane allowable of $1.5S_m = 233$ Mpa.

The fatigue allowable for interlaminar shearing stress between copper conductor and impregnated insulation is based off of the final test report from the manufacturer, Composite Technology Development. The conductor surfaces for these short beam shear specimens were sandblasted and primed, and were half lapped before impregnation with fiber glass cloth; however, they did not include Kapton tape interleaved with the glass cloth.

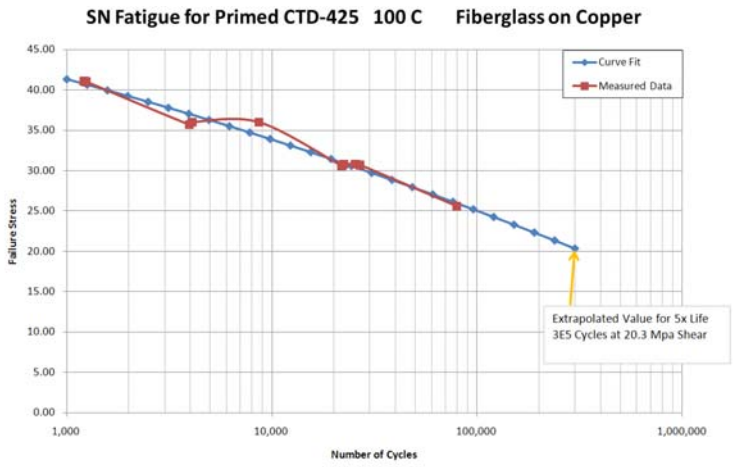

Although not included in the series of testing, the ultimate tensile strength for G10 or impregnated insulation is dominated by the strength of the glass reinforcement, and is typically higher than 200 Mpa.

3.0 Geometry / Modeling Assumptions

Geometry for the 3D finite element analysis was imported into Ansys directly from the Pro/Engineer solid models which were used to generate engineering drawing. Modifications were then made in Ansys Workbench Design Modeler to simply, defeature, and facilitate meshing. Element types 186 and 187 were used, which are 20 node bricks and 10 node tetrahedrons capable of electric, thermal, and structural degrees of freedom. However, these analyses were not coupled and simultaneously solved; rather the solution from one analysis type was imported as an initial condition into the next, in order to keep the model linear during structural and electric analyses. The mesh is a single continuous multibody part, predominately swept hexes in the conductor regions and coaxial cable insulation; bulk structural G10 in was modeled as tetrahedrons.

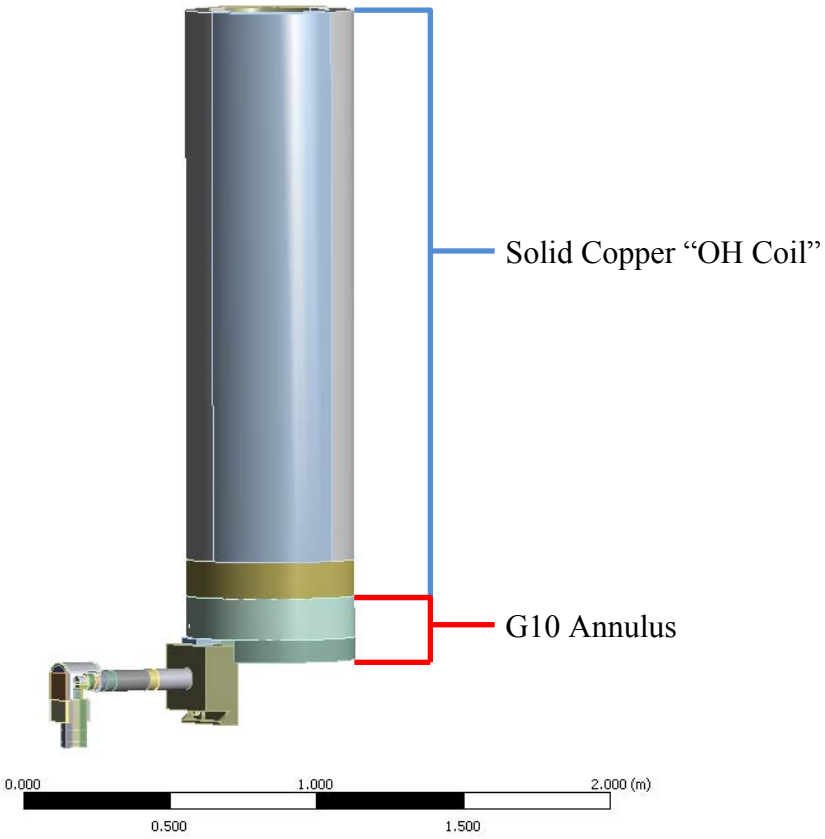

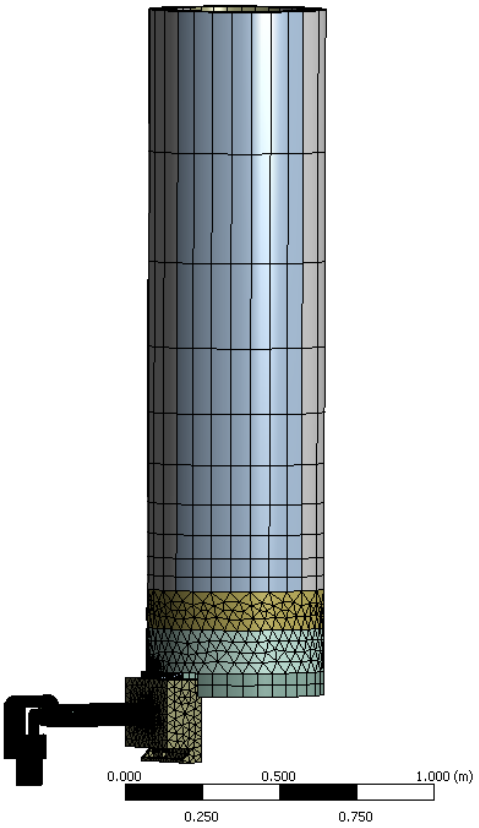

One key driving phenomena in the embedded leads region is the radial thermal expansion imposed on the G10 annulus from the main body of the OH Coil. In order to properly capture the distribution of this displacement along the top surface of the G10 annulus, a simplified representation of the OH coil, made of pure copper at the appropriate temperature, was included.

Inside of the G10 annulus, the embedded lead geometry is matched accurately in the region near the braze joint to the lead flags and the transition from vertical to tangential orientation. However, further away from this region of interest the two embedded leads were artificially joined together. In this way the conductor is properly anchored inside of the G10, and can develop realistic hoop stresses without modeling explicitly the helical winding as it transitions into the body of the coil. Furthermore, this simplification allow for a continuous conduction path during the electrical analysis.

The lead flags are modeled as completely encapsulated inside of a G10 box, with all surfaces flush, as if the box was impregnated with epoxy. In reality this box is fabricated out of several machined pieces of G10 which surround and interlock the lead flags. This simplification is valid, because the stress levels are extremely

low, provided that during assembly either a room temperature curing filler material is used to fill any remaining gaps, or that shims are used to prevent any motion of the lead flags.

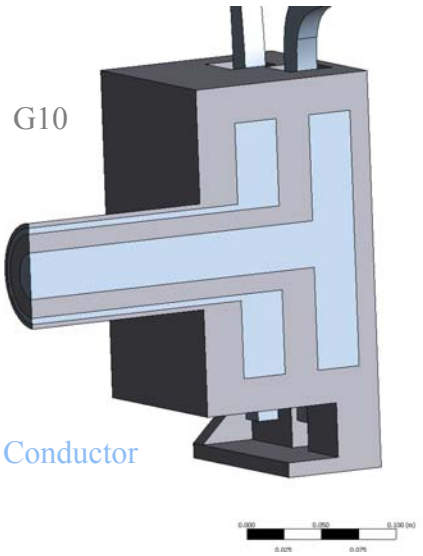

Cross Section Through Coax Box

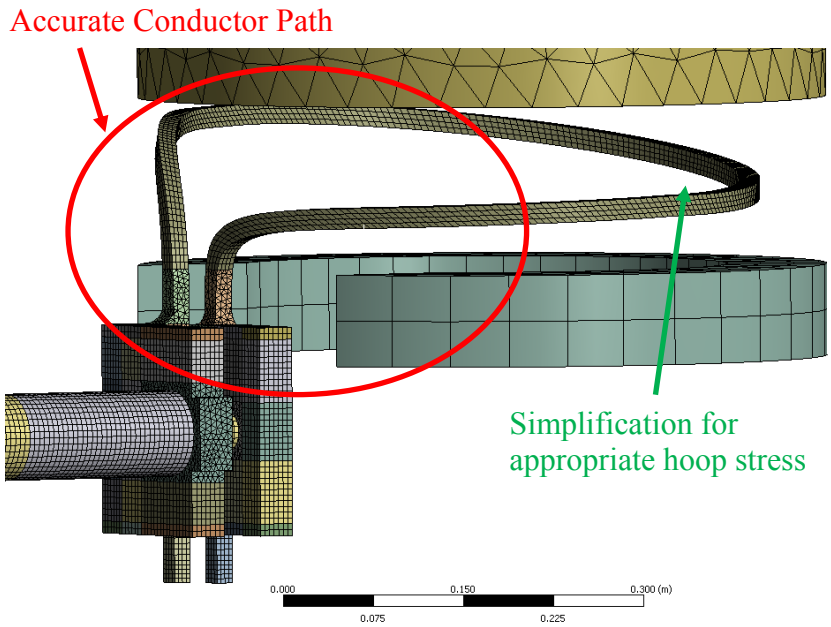

The section of conductor that "breaks through" through the G10 annulus as transitions into the coax box must be encapsulated inside of a filler material to prevent peaking stresses at structural discontinuities. It is recommended that a room temperature curing structural filler material, such as Henkel's Hysol, is used to fill these voids.

The model is extended to include the top several inches of the bus. At this cut boundary internal net reaction forces an moments can be applied from the bus bar calculation (NSTXU-Calc-55-01), far enough away from regions of interest to give accurate results.

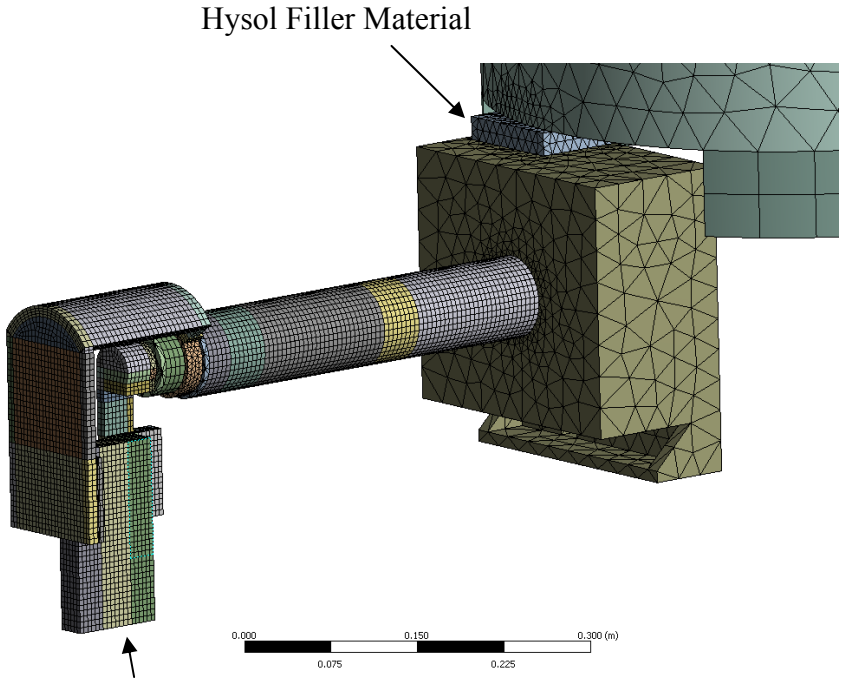

Cut Boundary Displacement

4.0 Updated Design, Electrical Analysis

A steady state electrical conduction analysis was performed to calculate actual current distribution over the conductor, which is especially important at regions of abrupt change in cross section. The conductor geometry, as shown in section 3, contains a continuous conduction path.

Although the General Requirements Document (GRD) specifies an equivalent square wave (ESW) of 24,000 Amps for a pulse length of 1.473 seconds, this is inconvenient to use in a transient thermal analysis due to the limitations on numerical stability, as detailed in section four. Therefore, a modified current of 7425 Amps was used, with the pulse length extended to 20 seconds, so that the same total Joule Heating was deposited.

Also, since the resistivity of copper is a function of temperature, but the thermal and electrical analyses were not coupled, an average value was used which yields the appropriate temperature at the end of the pulse.

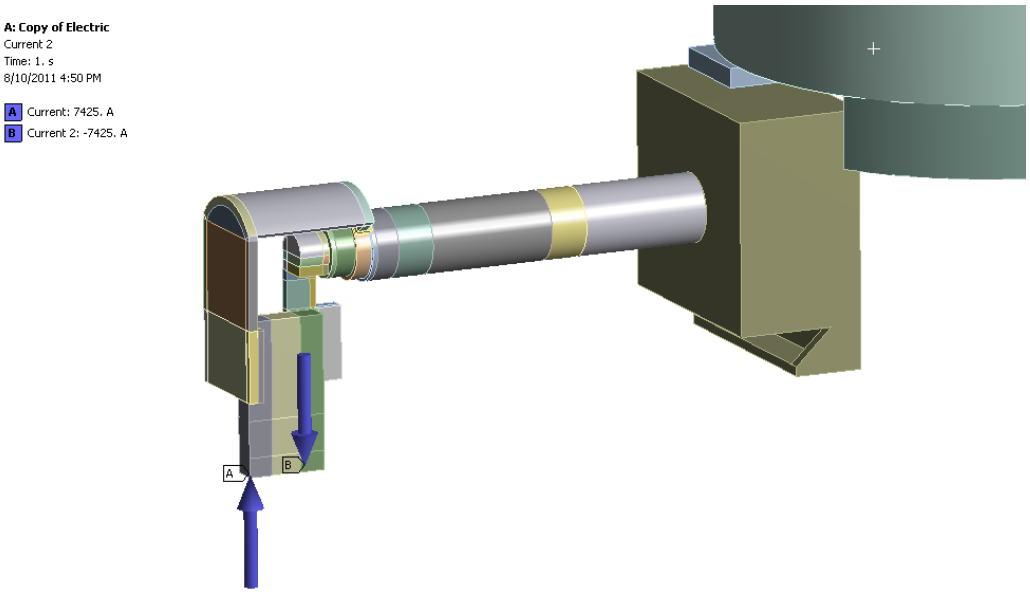

Applied Current on Conductor Cut Boundary at Bus Bar

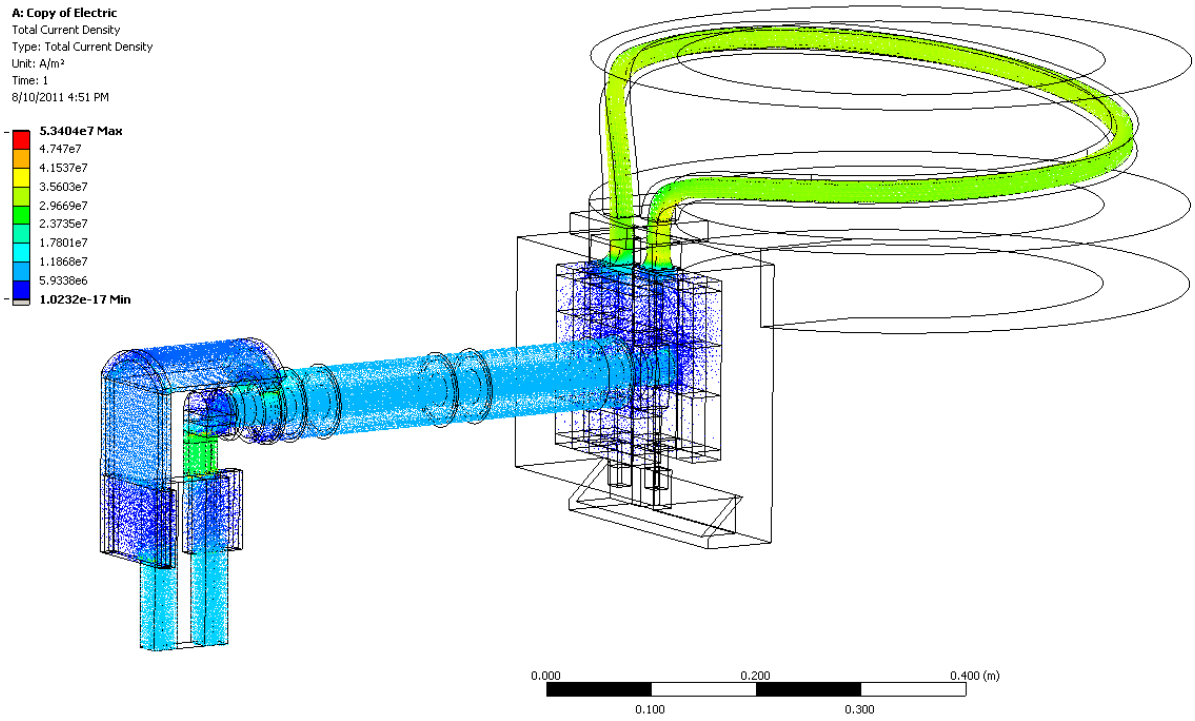

Current Density Vector Plot

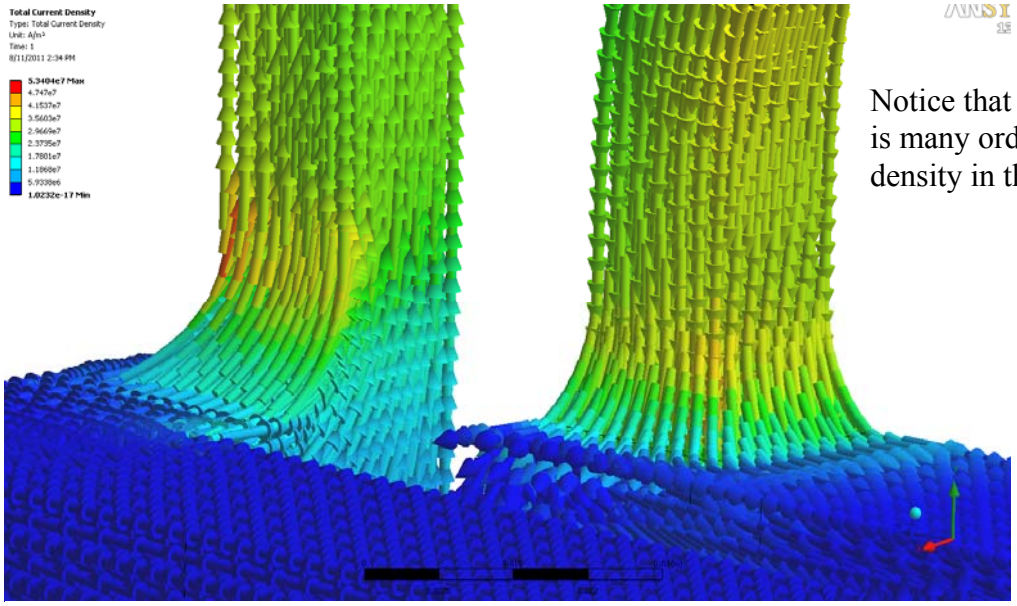

Notice that the current density in the lead flag is many orders of magnitude below the current density in the conductor.

Current Density Near Joint Between Conductor and Lead Flag

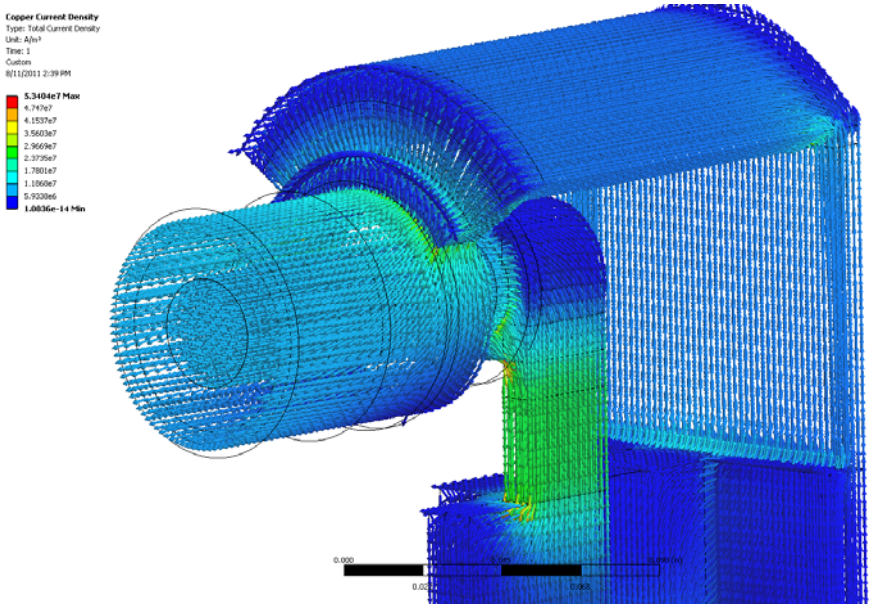

Current Density Near Coax/ Bus Bar

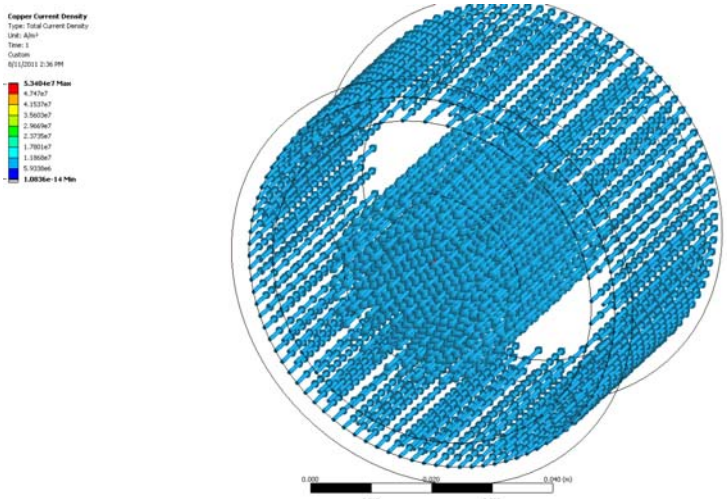

Current Density Vector Plot
Through Slice of Coaxial Cable

5.0 Updated Design, Thermal Analysis

The Joule heating calculated as a solution to the steady state electrical conduction model was imported as an initial condition into a transient thermal analysis to calculate smooth temperature distributions immediately after the pulse.

Numerical stability imposes a restriction on the element size vs. minimum allowable time step, shown below. Although the GRD specifies an ESW of 24kA for 1.473 seconds, the true pulse waveform is approximately 8 seconds long, with a varying current.

$$\Delta t \geq \frac{(\Delta x)^2}{4\alpha}$$

For G10 $\alpha \approx 1.3\text{E}-7$ and For Copper $\alpha \approx 1.1\text{E}-4$

$$G10 \qquad \Delta x \leq \sqrt{(4\alpha)(\Delta t)} \approx \sqrt{(4)(1.3\text{E}-7)(8)} = 0.002 \text{ m}$$

$$Cu \qquad \Delta x \leq \sqrt{(4\alpha)(\Delta t)} \approx \sqrt{(4)(1.1\text{E}-4)(8)} = 0.05 \text{ m}$$

We see that for a time step of eight seconds, the G10 requires an element length of 2 mm or smaller, whereas the copper only requires an element of 50 mm or smaller. This size difference is because of the three orders of magnitude differences in thermal diffusivity. In order to keep the solving time relatively short, a relatively large mesh size of 0.02 m is used in regions, especially of G10, that are not particularly interesting.

Since the primary purpose of this thermal analysis was not to accurately represent the transient response, but rather to calculate smooth temperature distributions at regions of abrupt changes in cross section in the copper conductor, a single time step of 20 seconds was used. An ESW which has a current of 7425 Amps for 20 seconds results in the same final temperature distribution. . This is a slightly higher current than would be calculated by the formula below, due to the single time step and modified resistivity. This time step is long enough to minimize the numerical error, but still short enough so that internal conduction within the copper does not artificially smooth out the temperature gradient.

$$I^2Rt = \text{Joule Heating Power}$$

$$I_2 = \sqrt{I_1^2\left(\frac{t_1}{t_2}\right)}$$

The correct distribution of Joule Heating on the conductor was imported directly from the electrical analysis. On the "mock" OH coil, an internal heating rate of 1.3E7 $\frac{W}{m^3}$ so that after the 20 seconds, the coil reached the appropriate temperature of ~ 94 C. All exterior surfaces are assumed to be adiabatic, and the initial temperature is 12 C – the inlet temperature of the cooling water. The effect of cooling water during the pulse is ignored.

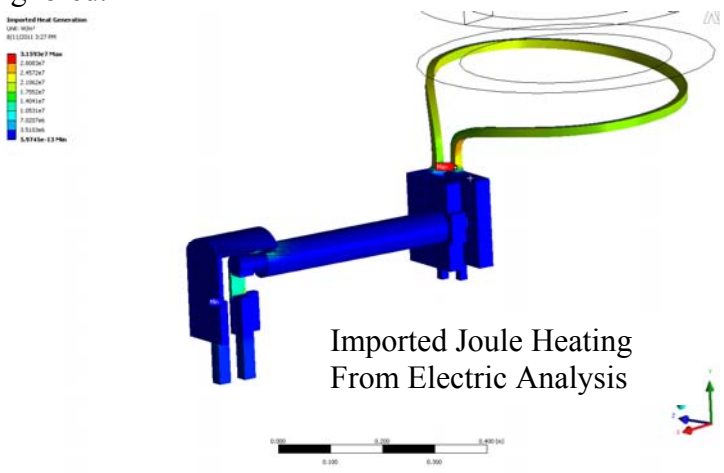

Imported Joule Heating
From Electric Analysis

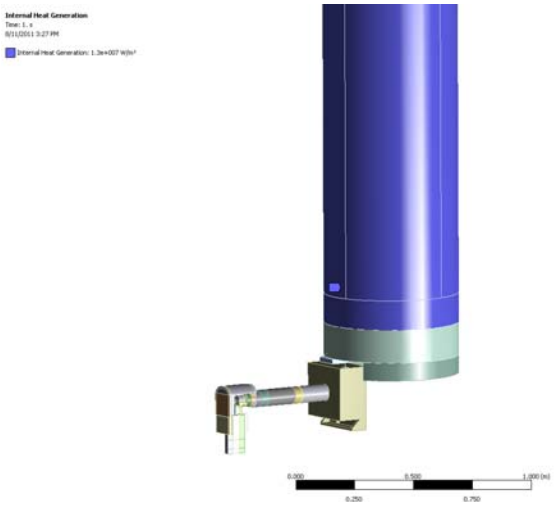

Applied Internal Heating On "Mock OH"

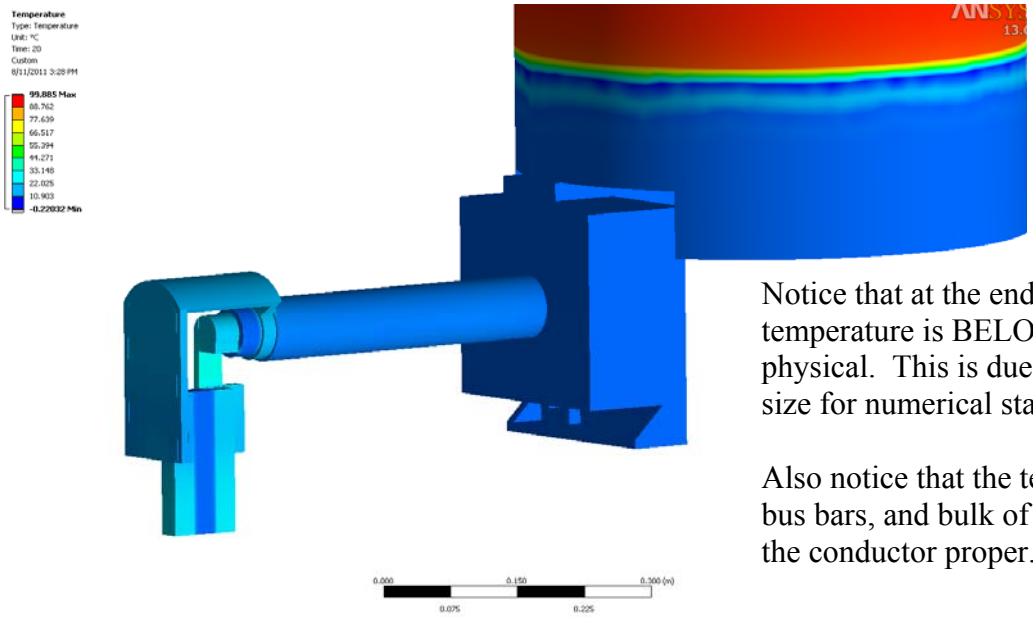

Temperature Distribution at End of Pulse

Notice that at the end of the pulse, the minimum temperature is BELOW the starting value, which is not physical. This is due to the limitations on element/step size for numerical stability

Also notice that the temperature rise inside the coax and bus bars, and bulk of the G10 is much less than inside the conductor proper.

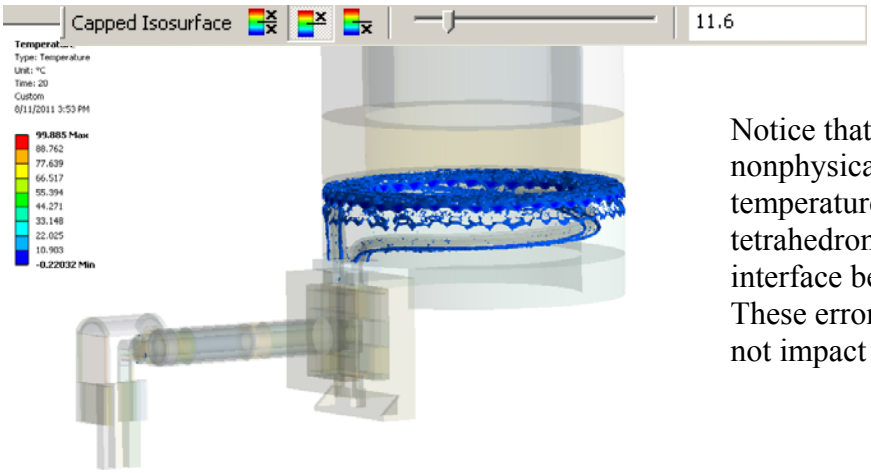

Elements which contain temperatures below 11.6 C

Notice that the regions containing nonphysical temperatures below the initial temperature are restricted to "large" tetrahedron elements of G10 near the interface between copper and insulation. These errors only affect small regions and do not impact stress results in important areas.

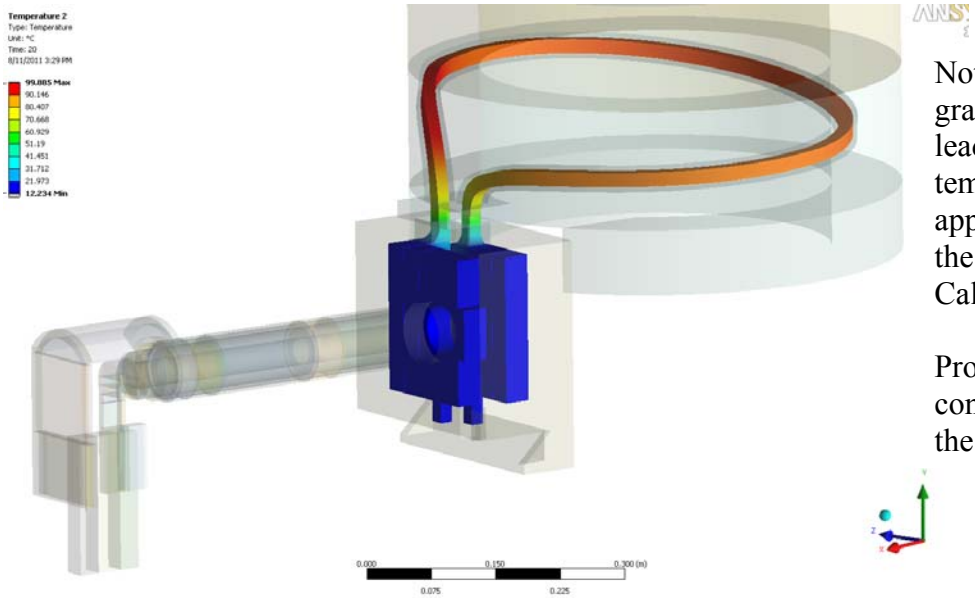

Temperatures at end of Pulse in Embedded Leads and Lead Flags

Notice there is a smooth temperature gradient near the transition between the lead flags and embedded leads. The temperature in the embedded leads is approximately 100 C, which matches the temperature calculated by NSTXU-Calc-133-06.

Provides this distribution as an initial condition to the structural analysis was the primary purpose of this model.

A second transient thermal calculation was performed to calculate the cooling between pulses. The results from the first transient analysis were imported as initial conditions. The effect of cooling water is modeled by imposing 12 C surface boundary conditions near the inlet of the coil. This is appropriate, because unlike in regions in the main body of the OH coil, near the inlet the water is always at approximately 12 C.

It is also assumed the active cooling will be implemented on the bus bars. This coolant should have the same inlet temperature as the coolant to the body of the OH coil to reduce thermal gradients across the coax. Furthermore, the water should flow in near the interface between the bus bars and the coaxial cable, and flow away from the machine, towards the power supplies. This maximizes the beneficial conduction between the coaxial cable and the bus bars.

Since coolant holes were not modeled in the bus bar, one outer surface of each bus bar conductor was modeled at 12 C constant surface temperature. All other exposed surfaces are modeled as adiabatic, neglecting any beneficial effect of convection to the environment. Auto time stepping was used, with step size varying between 6 seconds and 120 seconds for a period of 20 minutes.

With these conditions, there is sufficient conduction through the uncooled coaxial cable to the actively cooled bus bars and lead flags that all components can cool almost entirely cool down within 15 minutes, and any thermal ratcheting throughout the day is not significant.

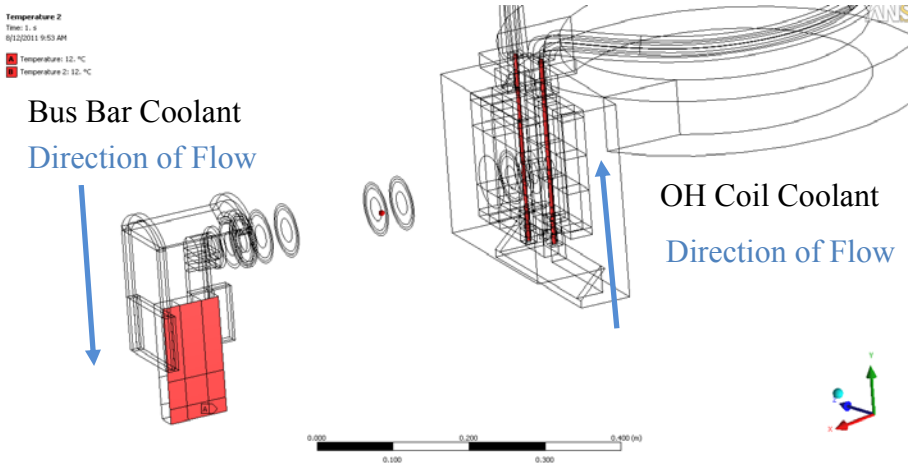

Constant Surface Temperatures of 12 C Representing Coolant Water

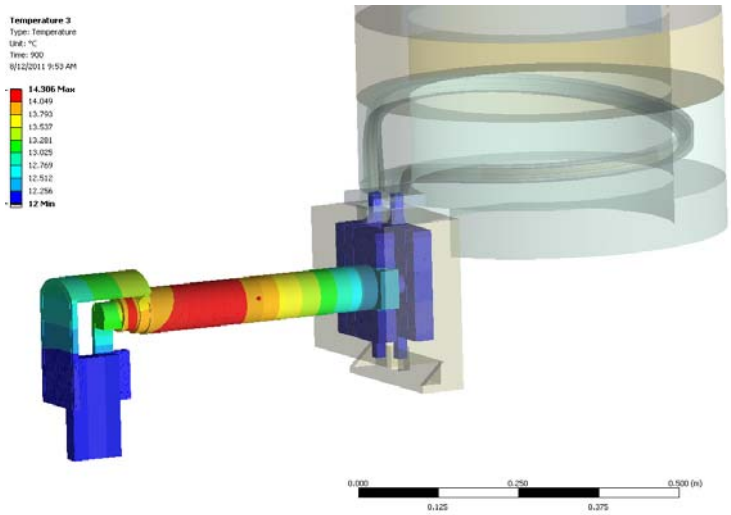

Coaxial Cable Temperature after 15 Minutes

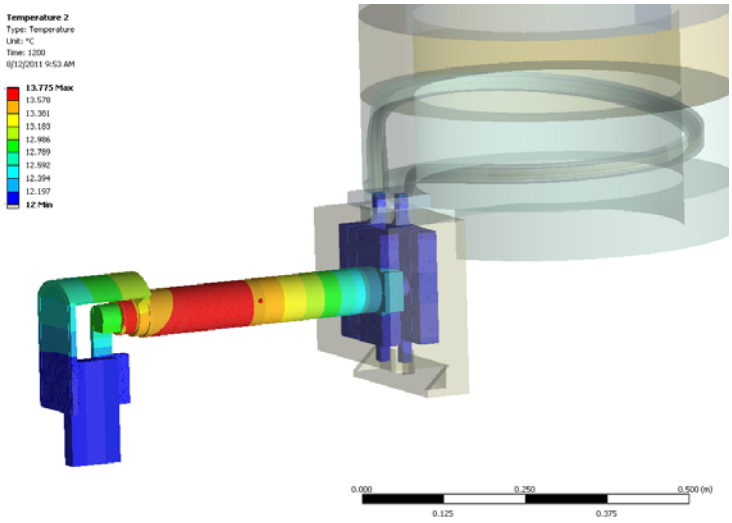

Coaxial Cable Temperature after 20 Minutes

6.0 Updated Design, Thermal Stress

The temperature distribution at the end of the pulse as calculated from the transient thermal analysis was imported into the static structural analysis. Fixed boundary conditions, as shown below, were imposed between the bottom of the G10 Annulus, where it is bolted to a steel support, at the exterior of the coax box, where it is shimmed inside of a steel cage, and at the interface between the top of the bus bar and the steel support clamp, which is mounted on the inside of the umbrella structure.

As detailed in Section 8, the support design for the bus bar is inadequate to absorb either the thermal expansion of the bus bars, or the torque created by the vertical current crossing the toroidal and radial fields. Therefore, for this analysis, it is assumed that the clamp will be redesigned to be many times stiffer, so that none of the reaction forces are absorbed by the coaxial cable, but are instead redirected towards the umbrella structure. This is represented by a fixed boundary at the clamping surface, and removes the need to include the internal forces at the cut boundary displacement.

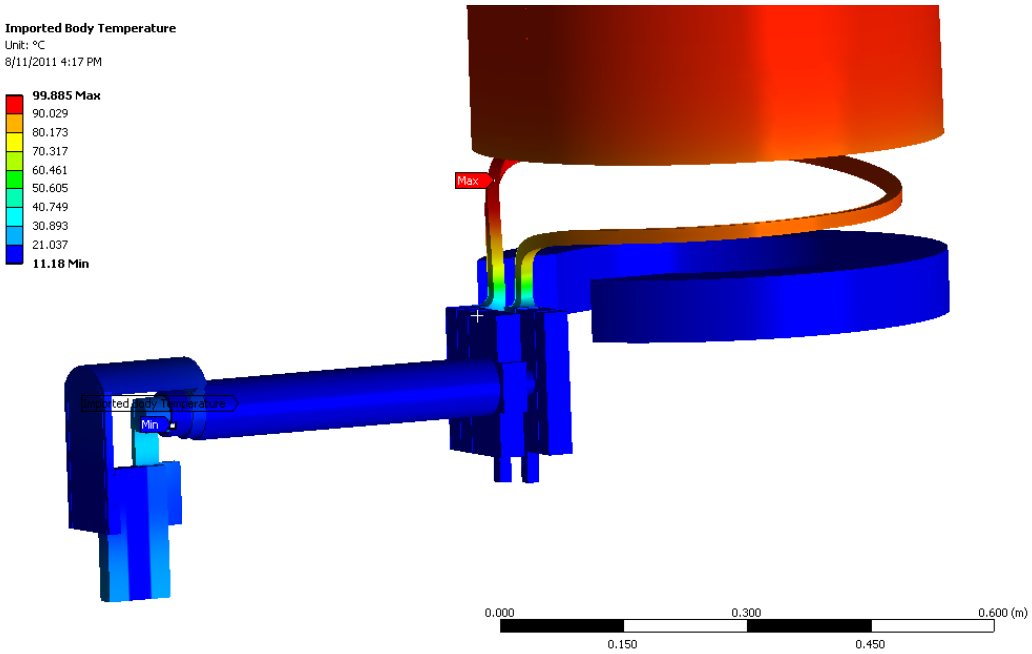

Imported Temperature Distribution

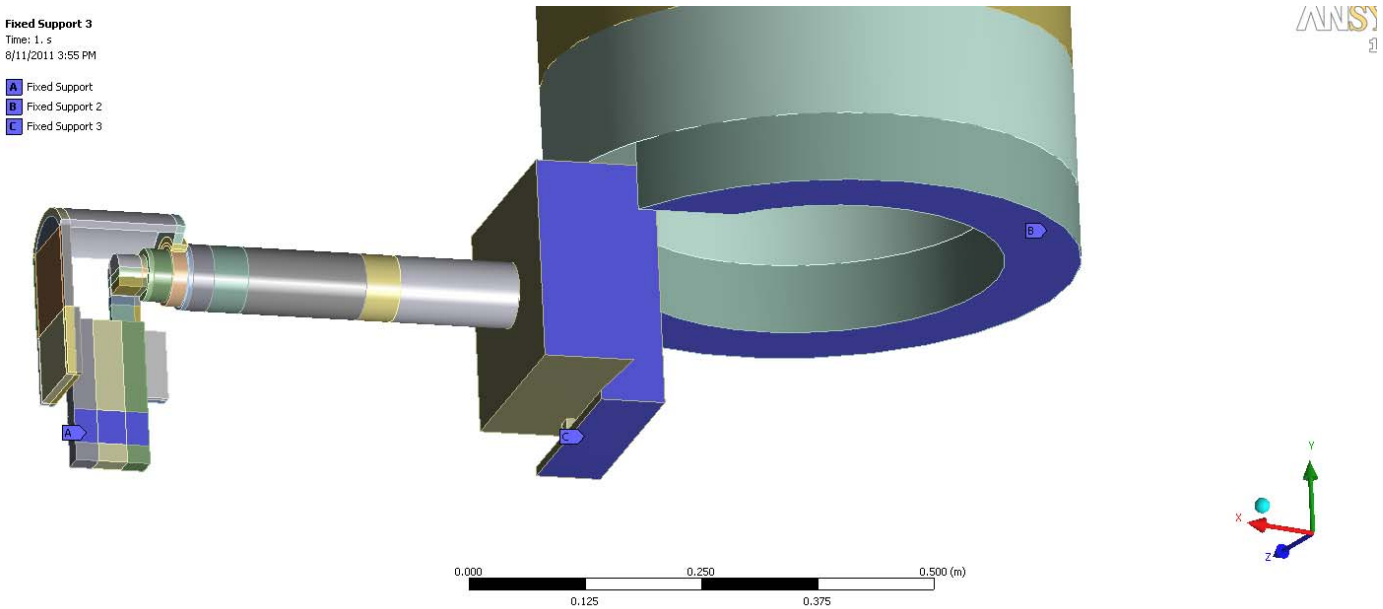

Fixed Support Boundary Conditions

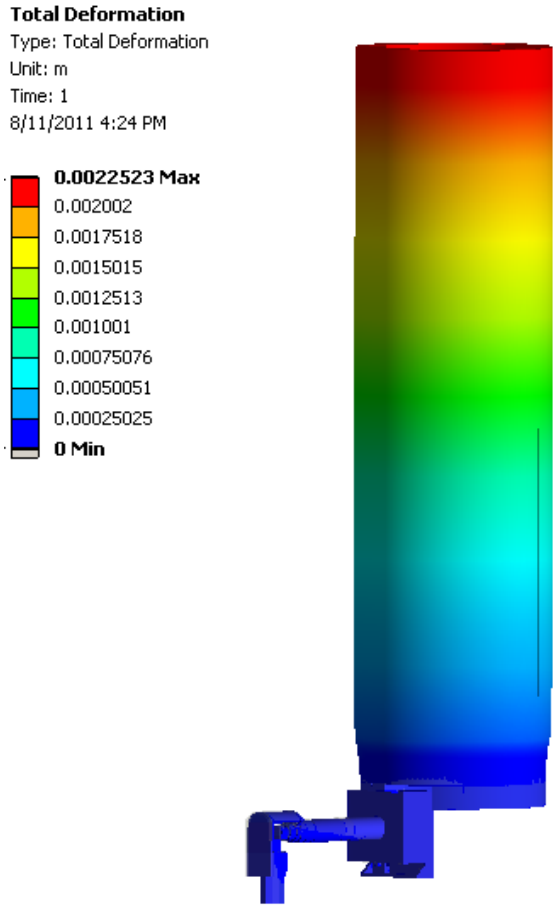

Notice that the coil is free to expand upwards, because of Belleville washers near the top

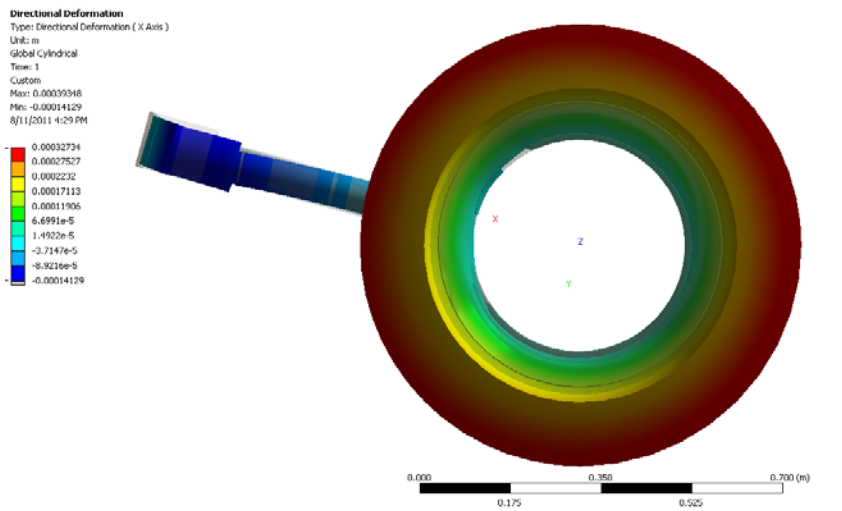

Radial Thermal Expansion at the Interface Between the Bottom of the Coil and the Top of the G10 Annulus

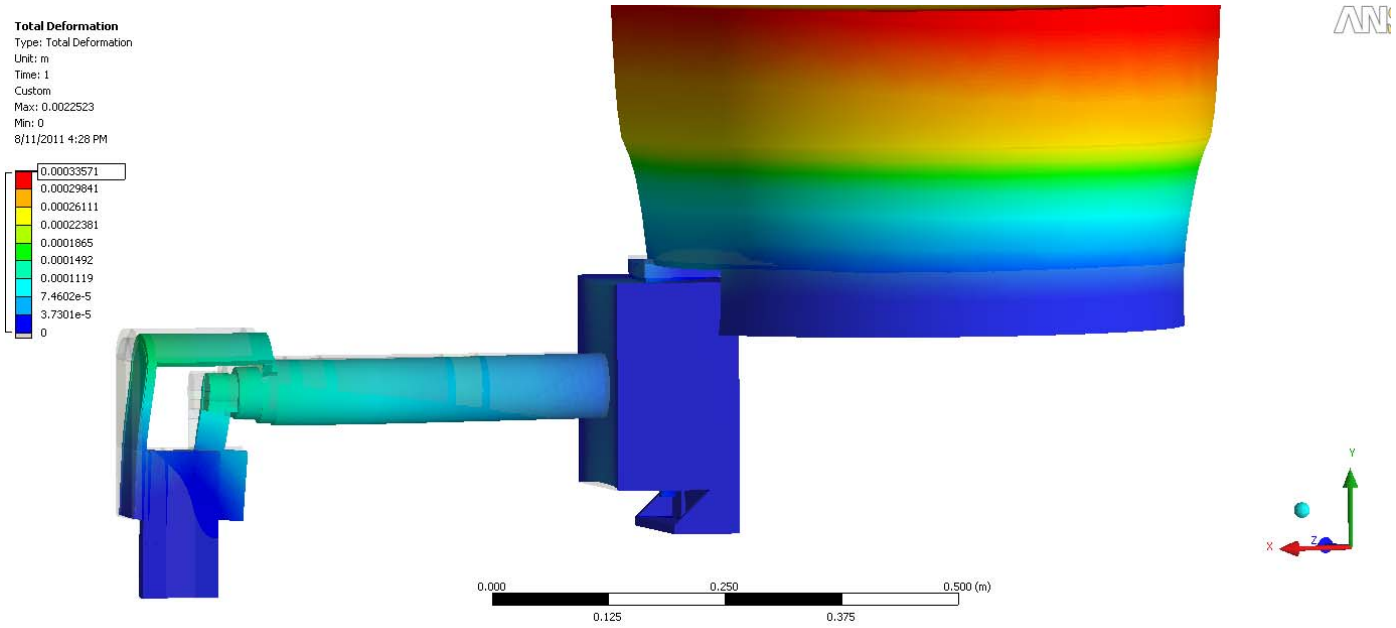

Total Deformation of the Coil

The differential between the thermal expansion of the copper, which is hot immediately after the pulse, and the G10 annulus, which remains cold is a major driver of stresses, especially in the embedded leads.

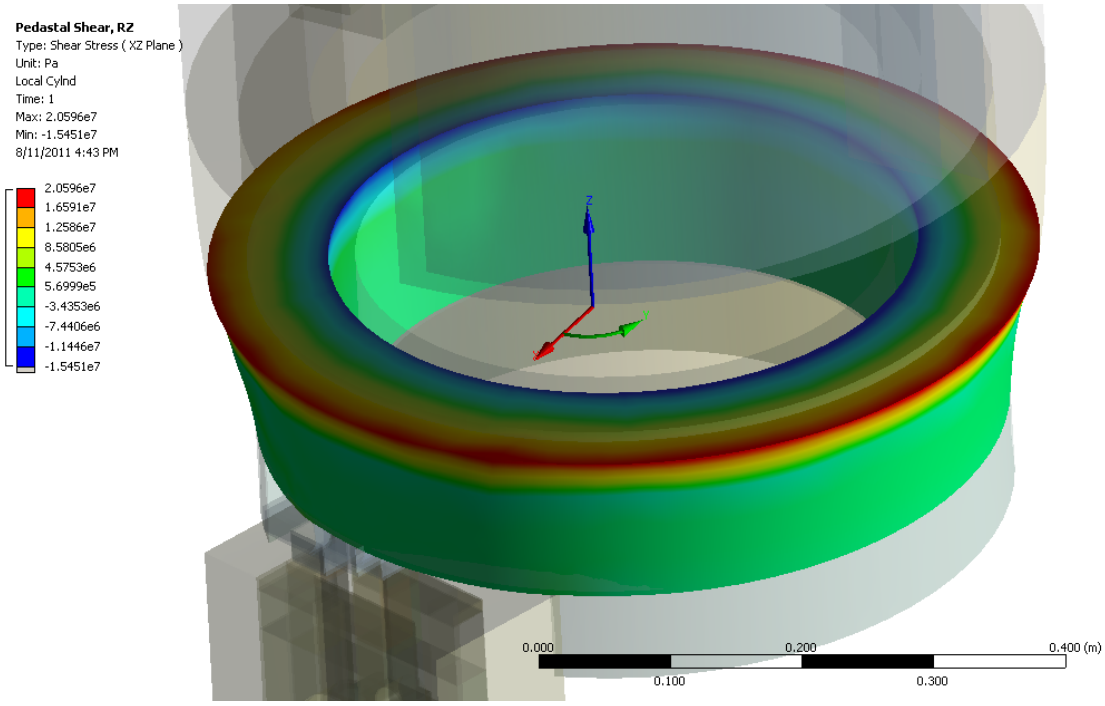

Shearing stresses on the RZ plane from differential thermal expansion.

In reality this interface is stepped due to the helical winding of the conductor, but Section 9 verifies the peak stresses are ~ 20 Mpa. To accommodate these, several turns of each conductor which are near this interface should be sandblast and primed to increase lamination strength. These stresses are below the 5x life requirement as extrapolated from test samples, once the knockdown factor is applied for interleaved Kapton. Local delamination is acceptable – see section 9.

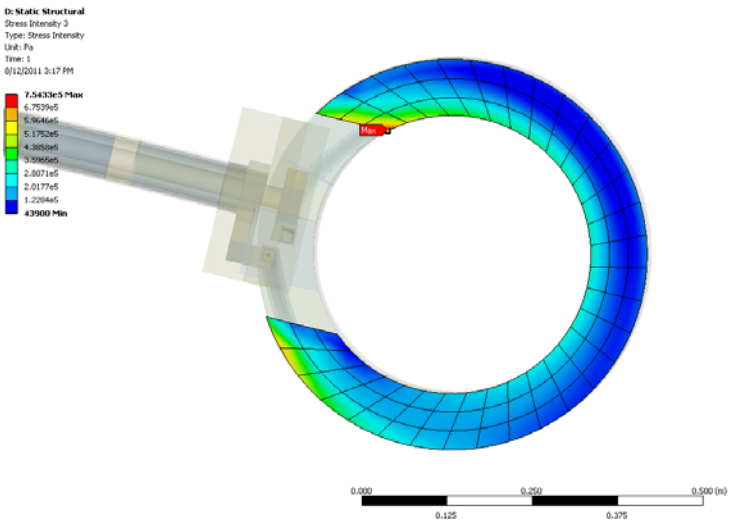

Stress Intensity at Bolted Interface
Between Bottom of G10 Annulus and Steel Support

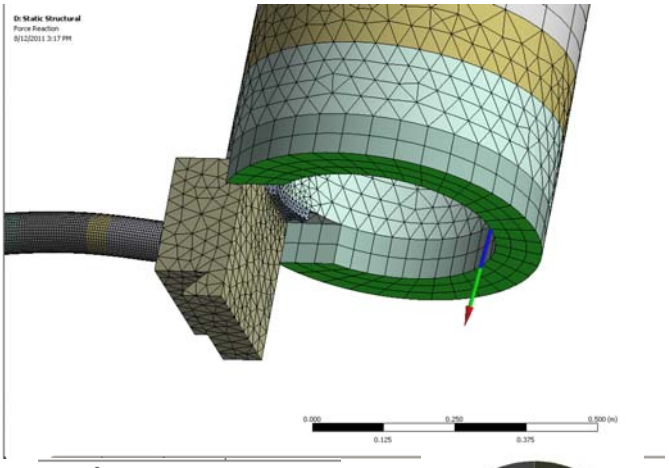

Results	
Maximum Value Over Time	
X Axis	1592.7 N
Y Axis	-15213 N
Z Axis	3749.2 N
Total	15749 N

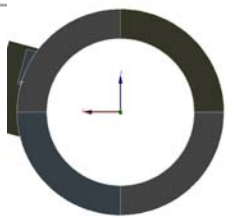

Total Reaction Forces at Bolted Interface

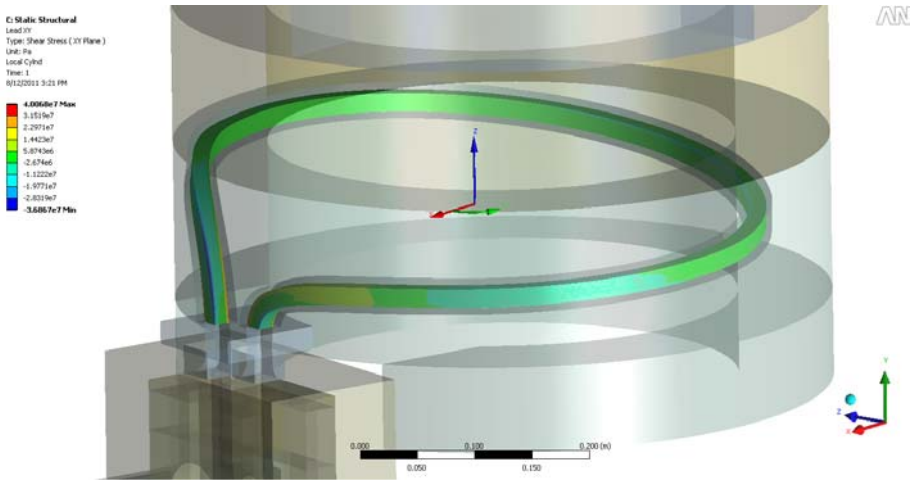

Shearing Stresses on Embedded Leads, R Theta

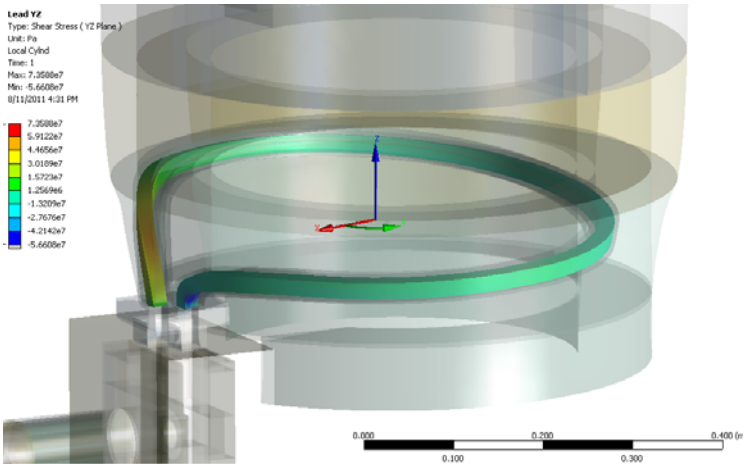

Shearing Stresses on Embedded Leads, Z Theta

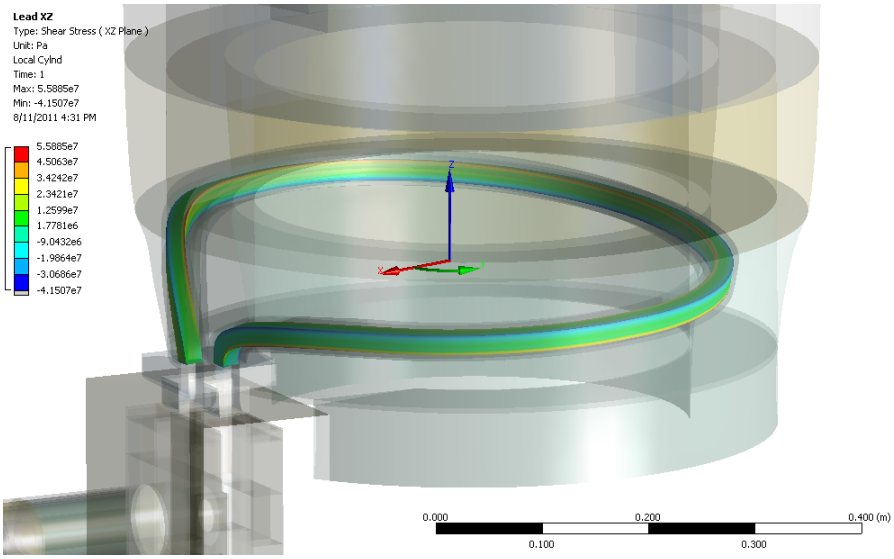

Shearing Stresses on Embedded Leads, R Z Plane

Delaminating shearing stresses on embedded leads peak at values higher than 50 Mpa, and will likely delaminate. However, because of the repeatable benign debonding at the copper/insulation interface, and the vast bulk of G10 surrounding the embedded leads, which will provide structural stability and insulating capacity, this is acceptable.

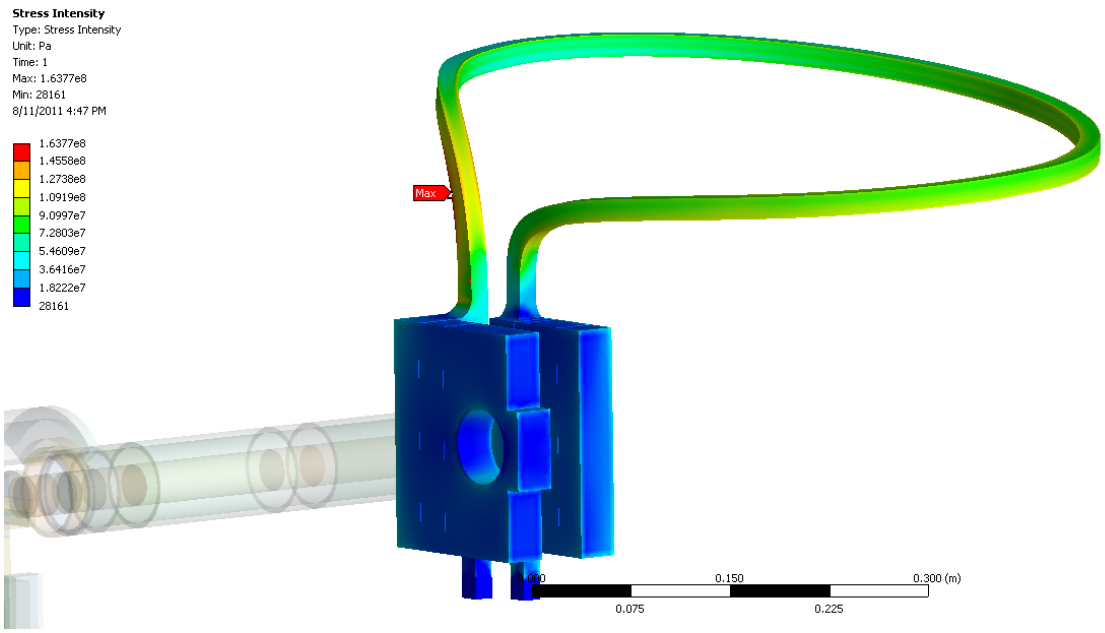

Stress Intensity in the Embedded Leads

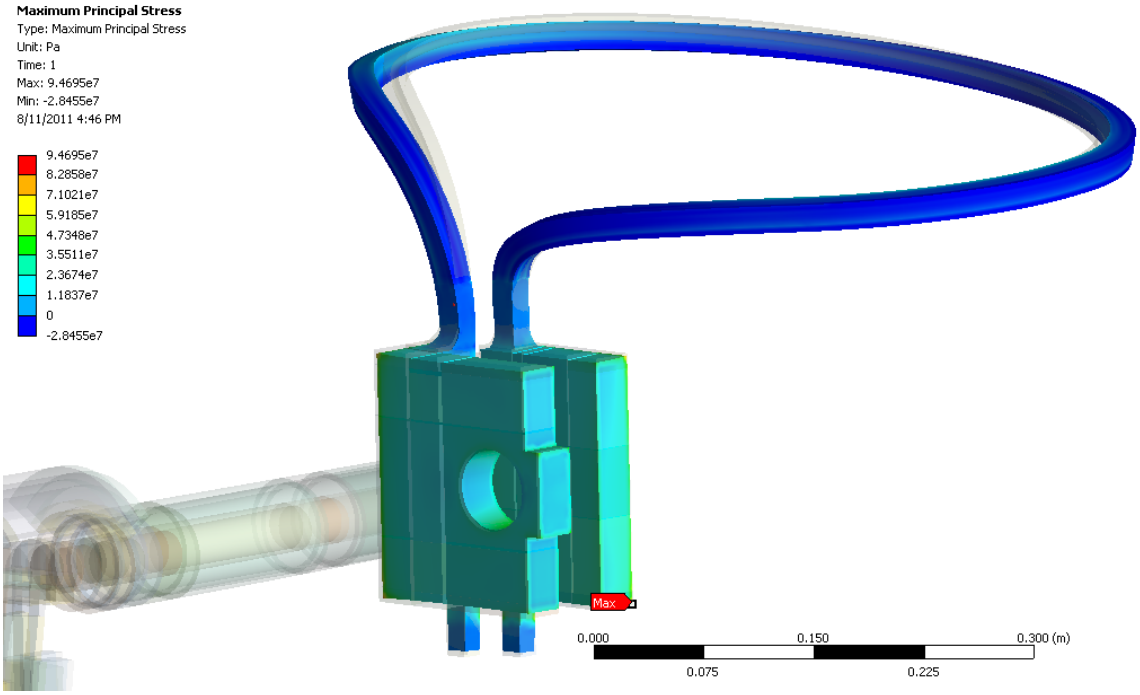

Max Principal Stress in the Embedded Leads

Since the max principal stress in the leads and flags is below the fracture mechanics evaluation requirement of 125 Mpa, the stress intensity needs only to meet static allowable. Except for a spurious concentration at a corner modeled with a sharp edge, the tensile principal stresses are exceedingly low, in fact primarily compressive within the leads. This is driven by the necessary addition of a fillet at the lead/flag braze joint, and the encapsulating structural filler material (ie Hysol) surrounding the conductor in the region between the G10 annulus and the lead coax box.

The static allowable (Sm) for the OH conductor is 157 Mpa. Note that the membrane stress is < 120 Mpa, and peak stress intensity is well below the allowed 235 Mpa (1.5 Sm).

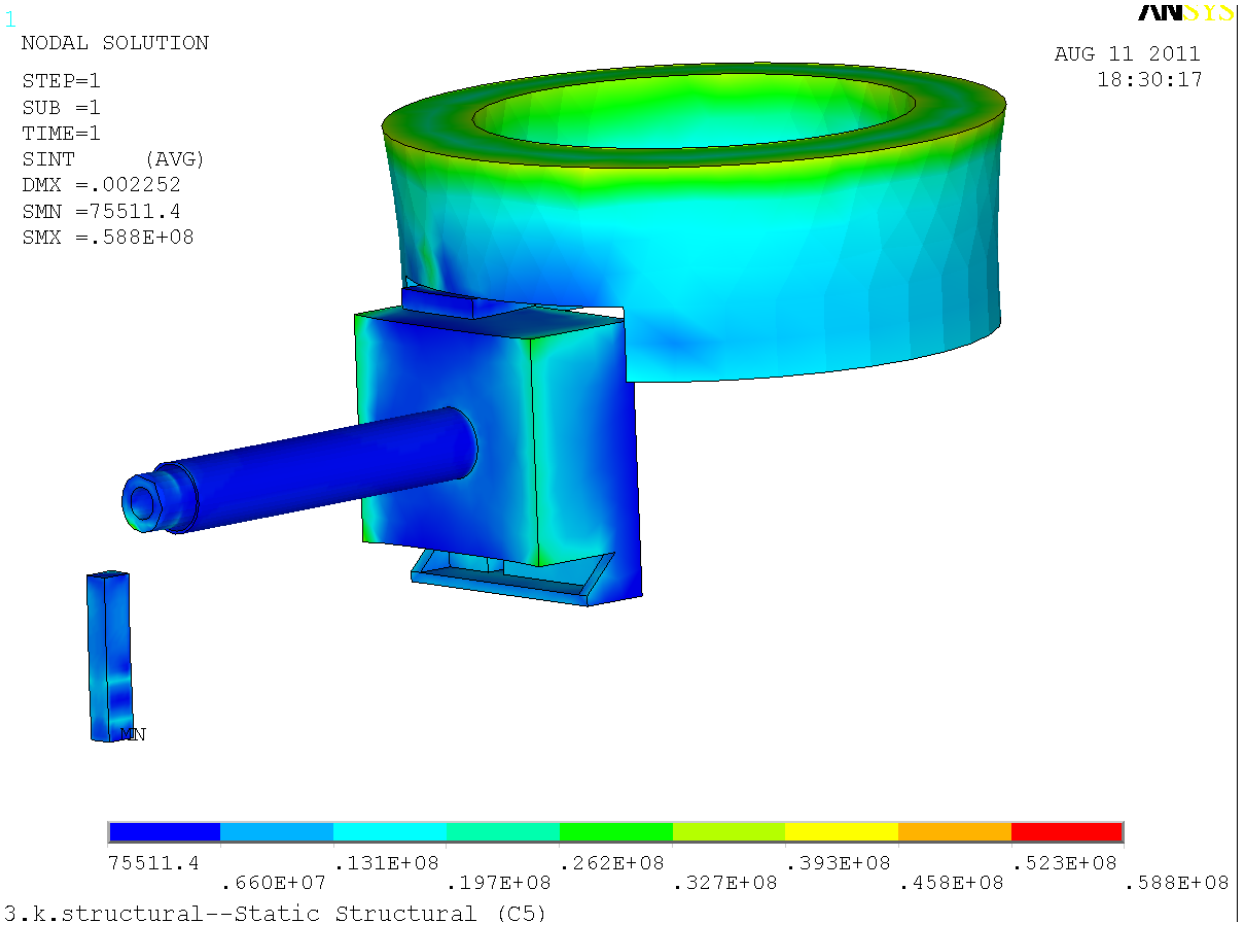

Stress Intensity in G10

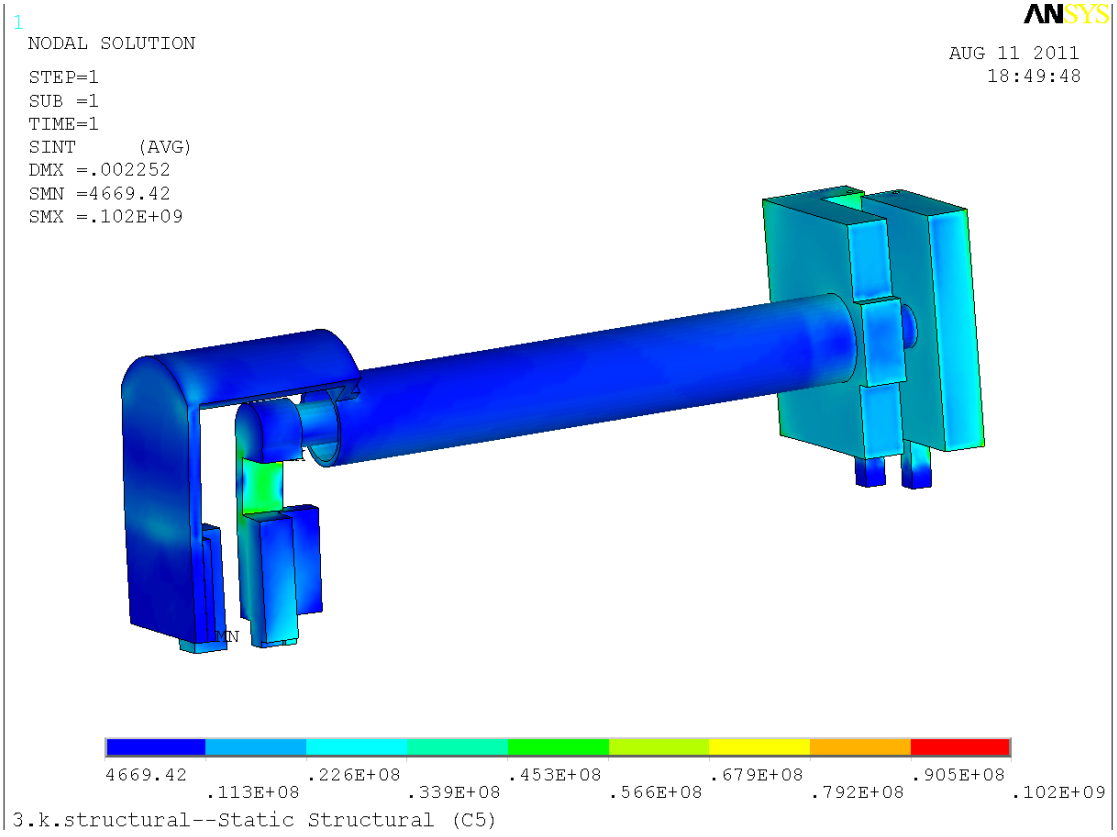

Stress Intensity Coaxial Conductor, Electrical Jumpers, and Lead Flags

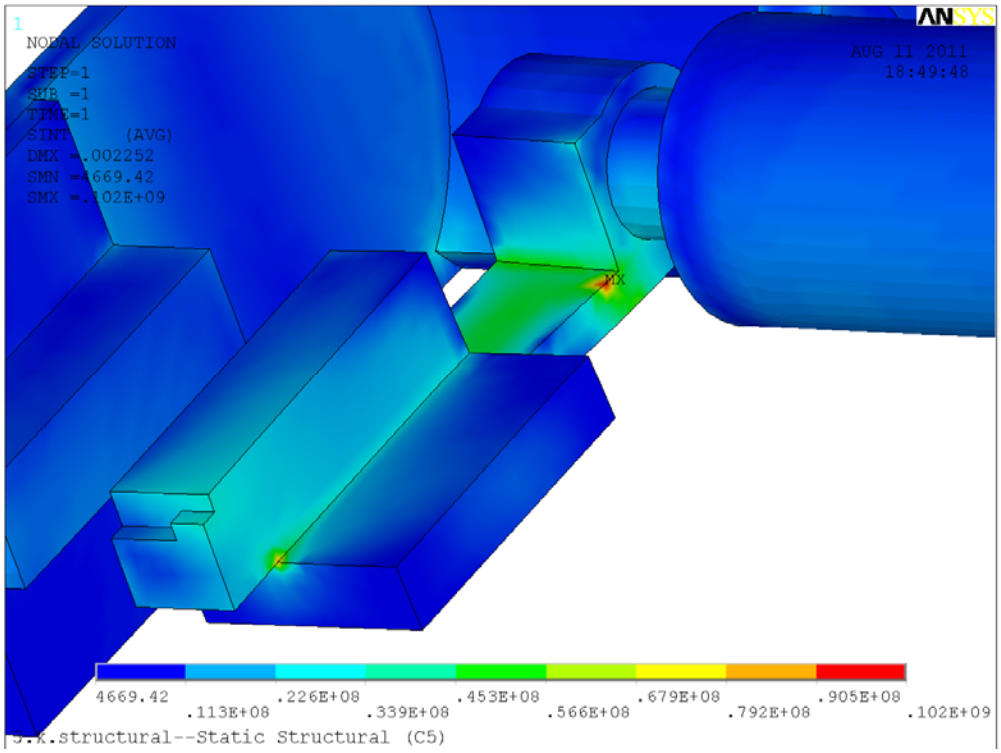

Stress Intensity in Coaxial Conductors and Electrical Jumpers is very low, except for spurious peaks at corners modeled as 90 degrees, where it is still below static allowable and SN 2x Stress fatigue allowable.

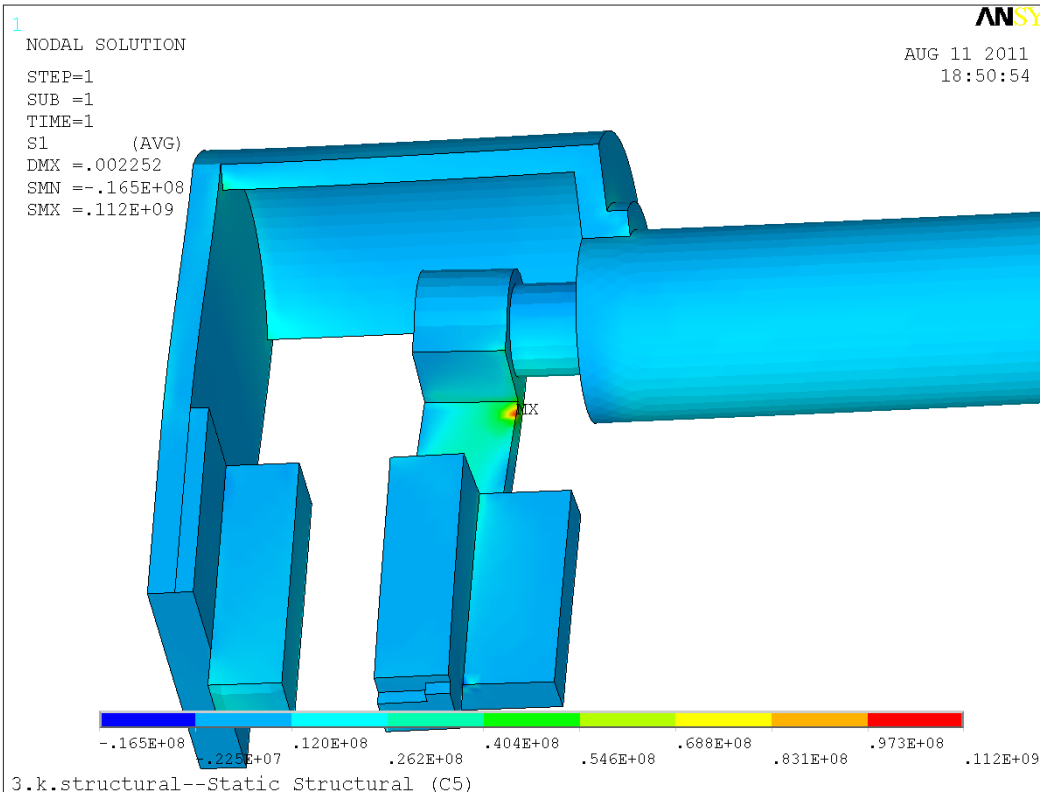

Max Principle Stresses in Coaxial Conductor, Electrical Jumper is below fracture mechanics fatigue allowable

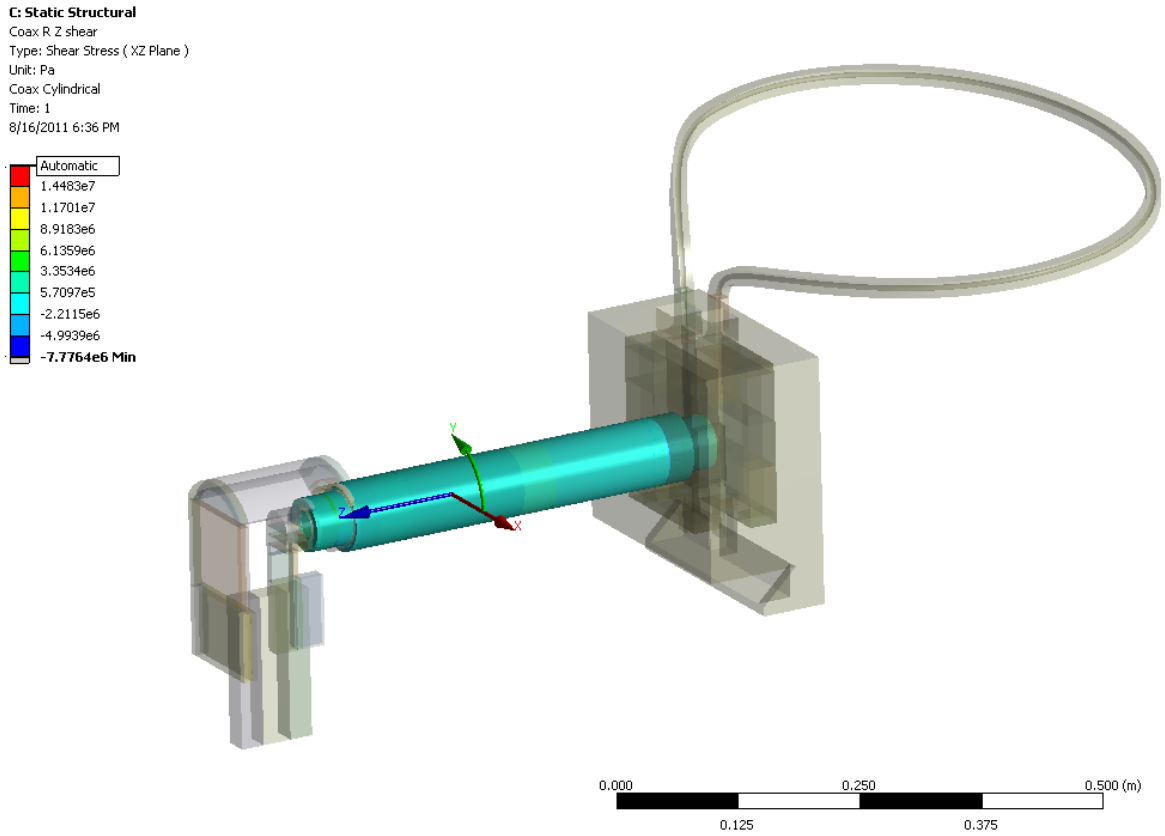

Shearing Stresses on Coaxial R Z Plane

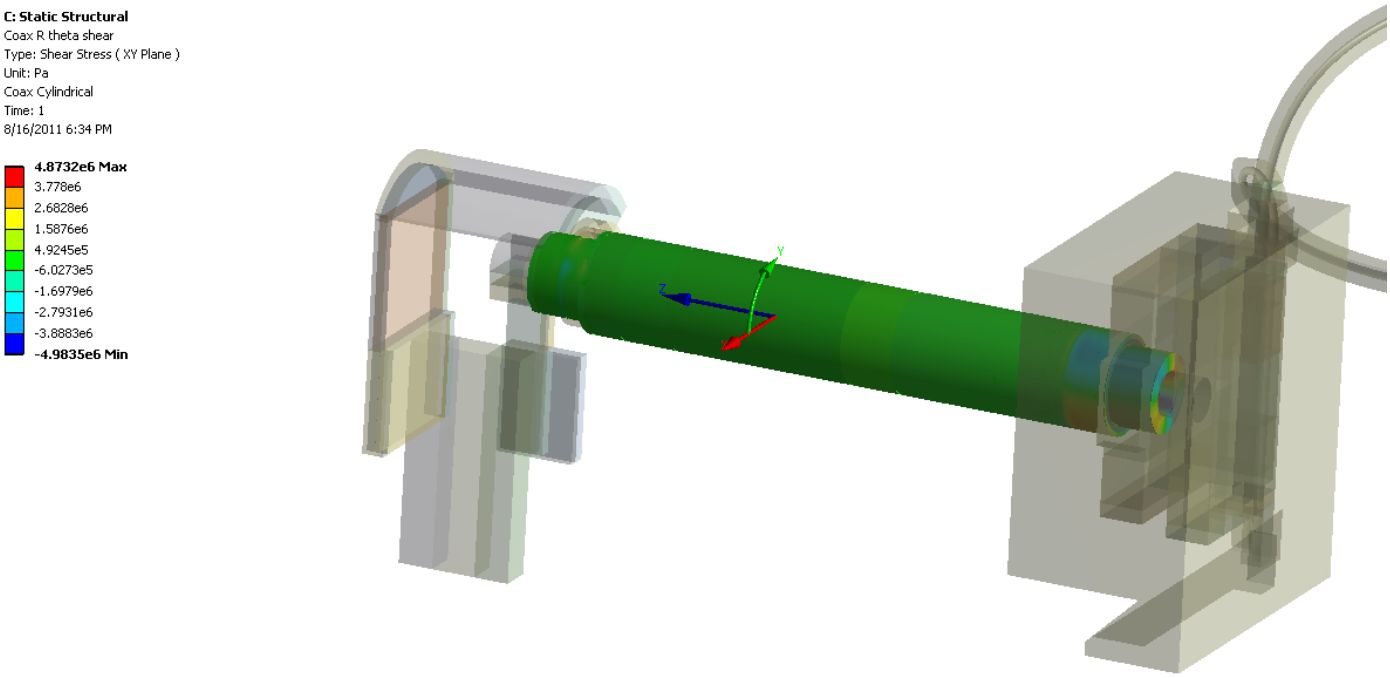

Shearing Stresses on Coaxial R Theta Plane

Shearing stresses on the coaxial cable from thermal effects are very low at the copper/insulation boundary. Peak Stresses shown on the coaxial insulation are fairly low, and it is unlikely that the coaxial cable will delaminate.

7.0 Lorentz Force Modeling and Results

Lorentz forces from magnetic fields equilibria were included in a separate model. First a MatLab script provided by Ron Hatcher (**NSTXU-CALC-13-01-00)** was used to determine which of the 96 scenarios listed in the GRD had the highest field values. This script is based on an analytical solution for the magnetic field from circular loops of current filaments. Multiple current filaments are used to represent the various Poloidal Field (PF) coils and a simplified representation of the plasma, and for a given point in space the radial and vertical fields are superimposed. Toroidal fields are calculated using a simple inverse radius relationship.

$$B_T = \frac{0.9344}{r} \quad \text{T}, \quad \text{r in meters}$$

Eleven representative points were chosen along one of the embedded leads, and for each of these points fields were calculated for the 96 different scenarios.

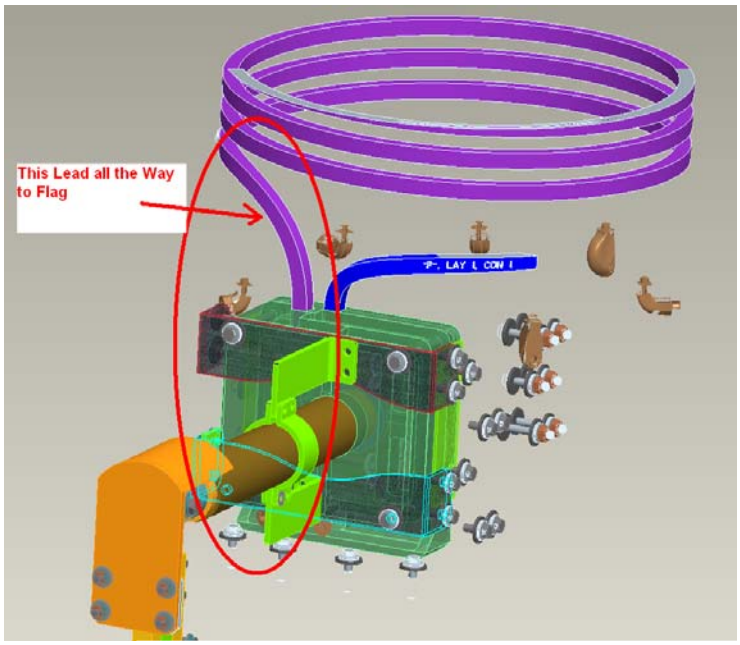

Location of Representative Lead

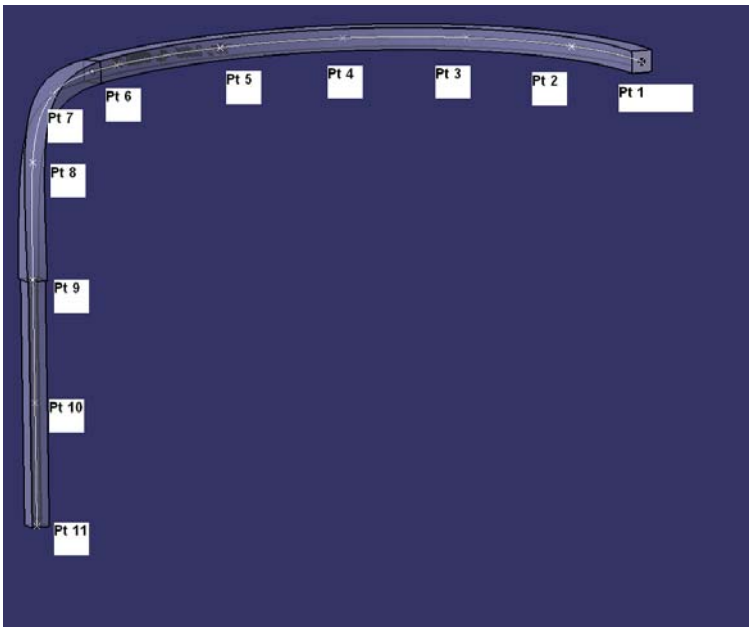

Eleven Equally Spaced Points where Fields Were Calculated

The vertical and radial fields for all 96 scenarios are plotted below. Notice that the vertical field is trimodal, because the vertical field is locally dominated by the OH coil (and there are three potential OH currents in the 96 reference cases). For a given scenario, the vertical field at all eleven point is almost exactly the same, because they are all at the same radius about the machine central axis, and the vertical field is not a strong function of height.

For the radial field, any given point will have a similar trimodal distribution depending on what the OH current is; however, unlike the vertical field the radial field is a strong function of height, and the points located before the lead conductor transitions downwards (Points Number 1-6) have a much radial higher field than those located further down.

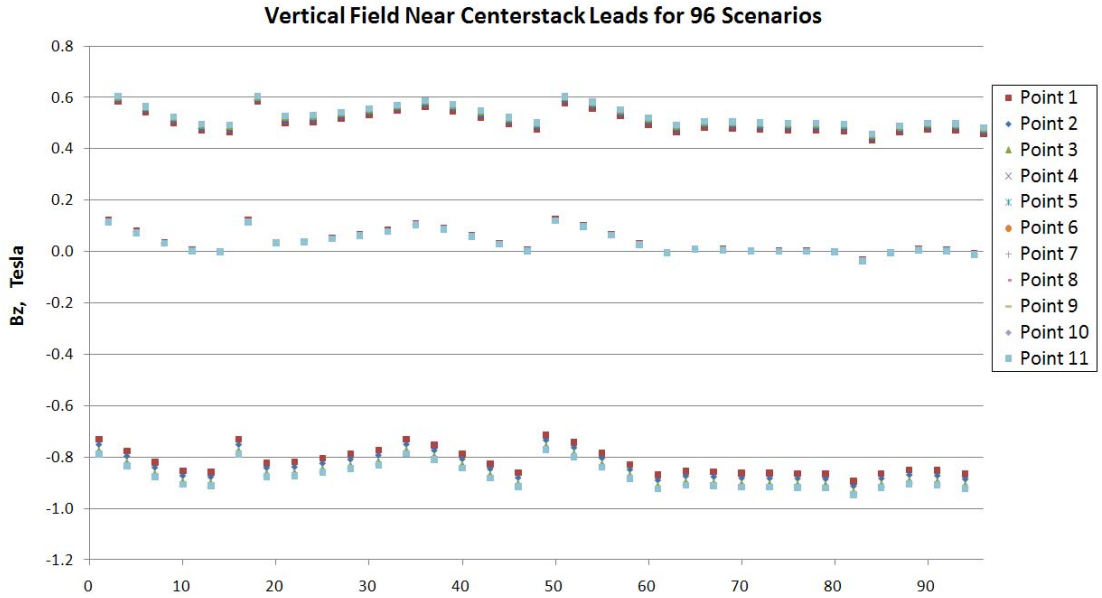

Vertical Fields In OH Coil Embedded Leads

Scenario 13

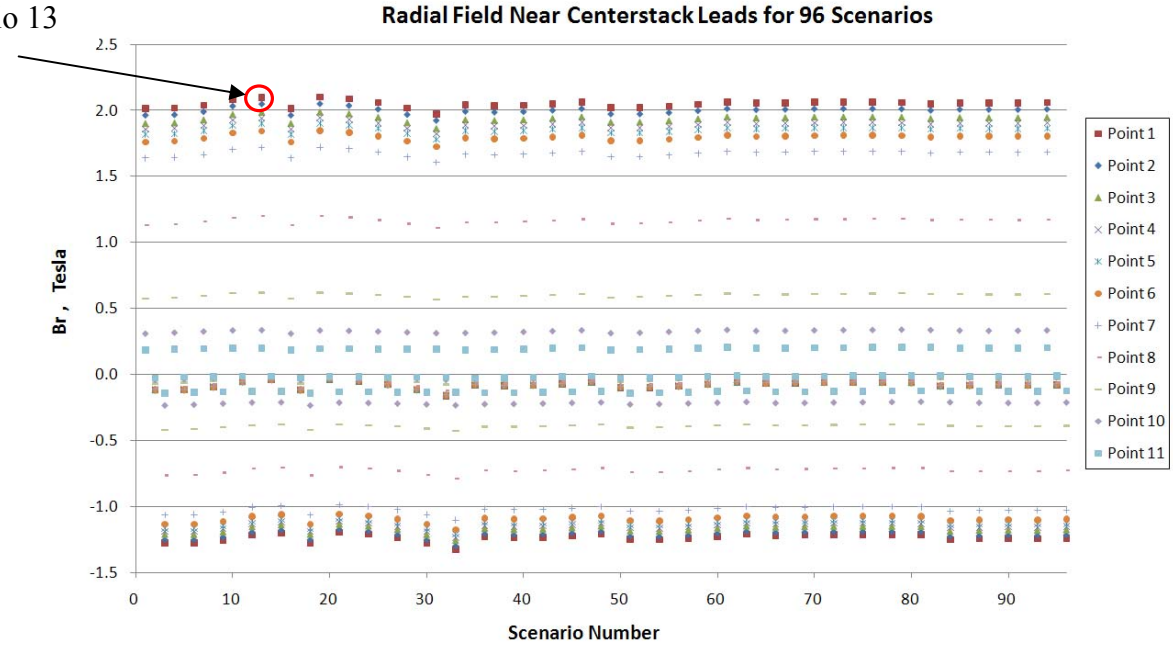

Radial Fields In OH Coil Embedded Leads

From this scoping we can see that the vertical and radial fields are dominated by the OH coil by virtue of their proximity. Scenario 13 was chosen as a representative bounding case.

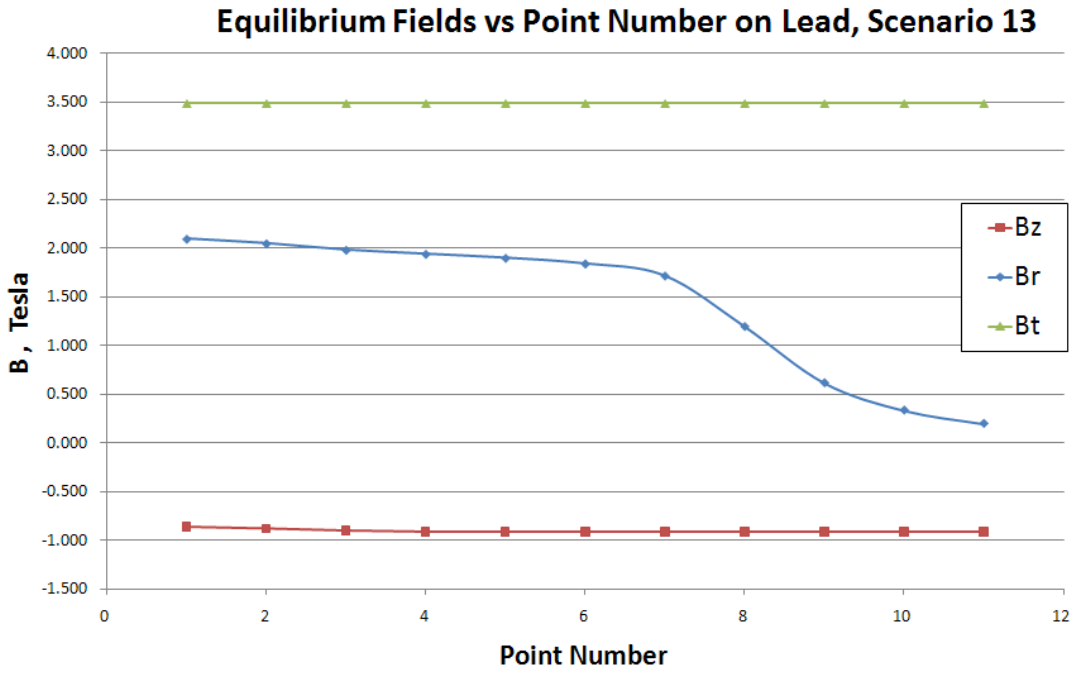

Magnetic Fields Along Embedded Lead for Representative Scenario

Three points along the coaxial cable were also chosen, and fields evaluated for Scenario 13. In this region, magnetic forces are less important because the coaxial cable is "forced balance" due to its equal and opposing currents, and because the field magnitudes are less.

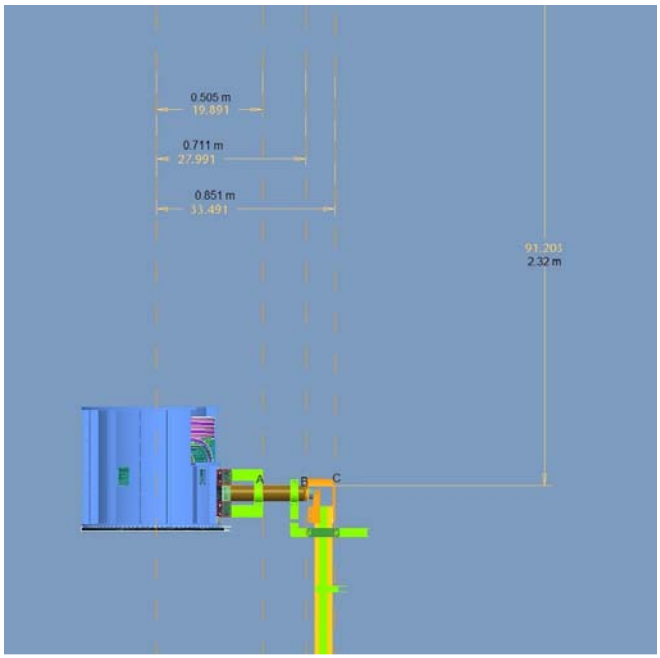

Three Representative Points Along Coaxial Cable

Magnetic Fields for Scenario 13 Along Coax						
Point	r (m)	z (m)	Br (T)	Bz (T)	Bt (T)	
A	0.505	-2.32	0.32	-0.31	1.85	
B	0.711	-2.32	0.188	-0.24	1.31	
C	0.851	-2.32	0.156	-0.23	1.1	

The magnetic fields computed from R. Hatchers Matlab script (**NSTXU-CALC-13-01-00)** for Scenario 13 close to the embedded leads were verified against values published by Robert Wooley (**Memo, R. Woolley, 17 December 2010)**. His values are tabulated below for 169 points, covering the same region with more resolution.

					Bz Near Coaxial Cable		meters, Telsas						
Z↓ (meters) R=	0.25	0.3	0.35	0.4	0.45	0.5	0.55	0.6	0.65	0.7	0.75	0.8	0.85
-2.1	-1.31	0.21	0.06	0.02	0.01	0.01	0.01	0.00	-0.01	-0.02	-0.05	-0.09	-0.13
-2.15	-1.18	-0.37	-0.17	-0.11	-0.07	-0.06	-0.05	-0.04	-0.05	-0.06	-0.08	-0.10	-0.12
-2.2	-1.01	-0.57	-0.33	-0.21	-0.15	-0.11	-0.09	-0.08	-0.08	-0.08	-0.09	-0.11	-0.12
-2.25	-0.85	-0.58	-0.39	-0.27	-0.20	-0.15	-0.13	-0.11	-0.10	-0.10	-0.11	-0.11	-0.12
-2.3	-0.72	-0.54	-0.40	-0.30	-0.23	-0.18	-0.15	-0.13	-0.12	-0.12	-0.12	-0.12	-0.12
-2.35	-0.61	-0.49	-0.39	-0.31	-0.25	-0.20	-0.17	-0.15	-0.14	-0.13	-0.13	-0.12	-0.12
-2.4	-0.53	-0.44	-0.36	-0.30	-0.25	-0.21	-0.18	-0.16	-0.15	-0.14	-0.13	-0.13	-0.13
-2.45	-0.46	-0.39	-0.34	-0.29	-0.24	-0.21	-0.19	-0.17	-0.15	-0.14	-0.13	-0.13	-0.13
-2.5	-0.40	-0.35	-0.31	-0.27	-0.24	-0.21	-0.19	-0.17	-0.15	-0.14	-0.14	-0.13	-0.12

Vertical Fields Near Coaxial Cable for Scenario 13, Wooley

					Br Near Coaxial Cable		meters, Teslas						
Z↓ (meters) R=	0.25	0.3	0.35	0.4	0.45	0.5	0.55	0.6	0.65	0.7	0.75	0.8	0.85
-2.10	2.22	1.47	0.95	0.68	0.52	0.40	0.31	0.23	0.17	0.12	0.08	0.05	0.05
-2.15	2.00	1.41	0.94	0.67	0.51	0.39	0.30	0.24	0.18	0.14	0.10	0.08	0.07
-2.20	1.21	1.03	0.79	0.61	0.47	0.37	0.29	0.23	0.19	0.15	0.12	0.10	0.09
-2.25	0.82	0.75	0.63	0.52	0.42	0.34	0.28	0.23	0.18	0.15	0.13	0.11	0.10
-2.30	0.58	0.55	0.50	0.43	0.36	0.30	0.25	0.21	0.18	0.15	0.13	0.12	0.11
-2.35	0.42	0.42	0.39	0.35	0.31	0.27	0.23	0.20	0.17	0.15	0.13	0.12	0.11
-2.40	0.31	0.32	0.31	0.29	0.26	0.23	0.20	0.18	0.16	0.14	0.13	0.12	0.11
-2.45	0.24	0.25	0.25	0.23	0.22	0.20	0.18	0.16	0.15	0.13	0.12	0.11	0.11
-2.50	0.19	0.20	0.20	0.19	0.18	0.17	0.16	0.15	0.13	0.12	0.12	0.11	0.10

Radial Fields Near Coaxial Cable for Scenario 13, Wooley

					B Toroidal Near Coaxial Cable		meters, Teslas						
Z↓ (meters) R=	0.25	0.3	0.35	0.4	0.45	0.5	0.55	0.6	0.65	0.7	0.75	0.8	0.85
n/a	3.74	3.11	2.67	2.34	2.08	1.87	1.70	1.56	1.44	1.33	1.25	1.17	1.10

Toroidal Fields Near Coaxial Cable, 1/r Relation

For speed of computation, these values were fit by least squares to the functions below, which are much simpler than the true functions, which are linear combinations of series solutions to elliptic integrals.

$$B_r(r,z) = \frac{A}{r} + \frac{B}{z} + \frac{C}{rz} + Dr + Ez + Frz + G$$

A	B	C	D	E	F	G
-6.764	12.71	-16.28	12.81	-5.982	5.472	-8.713

$$B_z(r,z) = \frac{A}{r^2} + \frac{B}{z^2} + \frac{C}{rz} + \frac{D}{r} + \frac{E}{z} + Fr + Gz + Hr^2 + Iz^2 + J$$

A	B	C	D	E	F	G	H	I	J	K
-0.4387	10.76	9.463	7.548	-9.685	-1.757	11.86	-6.619	1.703	-6.745	1.501

The square of the error of these functions, in units of Tesla, are tabulated below. There is extremely good agreement, except for the vertical fields in a localized region. We shall see through comparison with an independent evaluation of the Lorentz force stresses, and the very low magnitude of these stresses that this approximation is more than adequate.

Br Error in Approximating Functions, Squared in Tesla													
Z↓ (meters) R=	0.25	0.3	0.35	0.4	0.45	0.5	0.55	0.6	0.65	0.7	0.75	0.8	0.85
-2.1	0.02	0.00	0.02	0.01	0.01	0.00	0.00	0.00	0.00	0.00	0.00	0.00	0.00
-2.15	0.07	0.03	0.00	0.00	0.00	0.00	0.00	0.00	0.00	0.00	0.00	0.00	0.00
-2.2	0.04	0.00	0.00	0.00	0.00	0.00	0.00	0.00	0.00	0.00	0.00	0.00	0.00
-2.25	0.09	0.01	0.00	0.00	0.00	0.00	0.00	0.00	0.00	0.00	0.00	0.00	0.00
-2.3	0.07	0.01	0.00	0.00	0.00	0.00	0.00	0.00	0.00	0.00	0.00	0.00	0.00
-2.35	0.03	0.00	0.00	0.00	0.00	0.00	0.00	0.00	0.00	0.00	0.00	0.00	0.00
-2.4	0.00	0.00	0.00	0.00	0.00	0.00	0.00	0.00	0.00	0.00	0.00	0.00	0.00
-2.45	0.01	0.00	0.00	0.00	0.00	0.00	0.00	0.00	0.00	0.00	0.00	0.00	0.00
-2.5	0.06	0.02	0.00	0.00	0.00	0.00	0.00	0.01	0.01	0.00	0.00	0.00	0.00

Error Squared in Approximating Function for Radial Field, Tesla

Bz Error in Approximating Functions, Squared in Tesla													
Z↓ (meters) R=	0.25	0.3	0.35	0.4	0.45	0.5	0.55	0.6	0.65	0.7	0.75	0.8	0.85
-2.1	0.09	0.45	0.07	0.01	0.00	0.00	0.00	0.00	0.00	0.00	0.00	0.00	0.00
-2.15	0.05	0.01	0.01	0.00	0.00	0.00	0.00	0.00	0.00	0.00	0.00	0.00	0.00
-2.2	0.01	0.01	0.00	0.00	0.00	0.00	0.00	0.00	0.00	0.00	0.00	0.00	0.00
-2.25	0.00	0.02	0.01	0.00	0.00	0.00	0.00	0.00	0.00	0.00	0.00	0.00	0.00
-2.3	0.00	0.01	0.01	0.00	0.00	0.00	0.00	0.00	0.00	0.00	0.00	0.00	0.00
-2.35	0.01	0.01	0.01	0.00	0.00	0.00	0.00	0.00	0.00	0.00	0.00	0.00	0.00
-2.4	0.02	0.00	0.00	0.00	0.00	0.00	0.00	0.00	0.00	0.00	0.00	0.00	0.00
-2.45	0.02	0.00	0.00	0.00	0.00	0.00	0.00	0.00	0.00	0.00	0.00	0.00	0.00
-2.5	0.02	0.00	0.00	0.00	0.00	0.00	0.00	0.00	0.00	0.00	0.00	0.01	0.01

Error Squared in Approximating Function for Vertical Field, Tesla

These analytical functions for radial, vertical, and toroidal fields for a representative bounding case can be used to compute and apply Lorentz forces directly to nodes in Ansys. The previous electric analysis, Section 4, has already calculated current density at every node throughout the mesh. The Lorentz force per unit length is equal to the current crossed with the magnetic field.

$$\frac{\vec{F}}{L} = \vec{I} \times \vec{B}$$

or equivalently

$$\vec{F} = LA\left(\vec{j} \times \vec{B}\right) \approx V\left(\vec{j} \times \vec{B}\right)$$

This can be rearranged to show that for a closed prismatic volume with constant current density parallel to the sides of the volume, the total force is equal to the volume times the current density crossed with magnetic field. This relationship implicitly assumed that volume is equal to cross section times length, which is only exact for properly aligned prismatic elements; however, this introduces only a small error for elements with aspects ratios close to one.

A Matlab script was written which imports nodal coordinates, element lists and volumes, and nodal current densities from Ansys. The volume of every element was then "assigned" proportionately to each of its non midside nodes, and magnetic fields computed at each of these nodes. In this way, every "corner" node has an appropriate volume, field, and current density, from which Lorentz forces were calculated, and imported into Ansys, and directly applied as nodal forces.

Some examples of applied nodal Lorentz forces are shown below. Notice that Lorentz forces are much higher in the embedded leads, where there is significant vertical compression and radial bursting loads. However, in this region the conductor is embedded entirely in a robust structure of G10. The region of most concern is the short vertical section of leads that transitions between the G10 annulus and the top of the lead flags. As shown below, it is recommended that this region be filled in with a structural bulking material, to absorb Lorentz forces, and to force thermal effects to resolve as compressive.

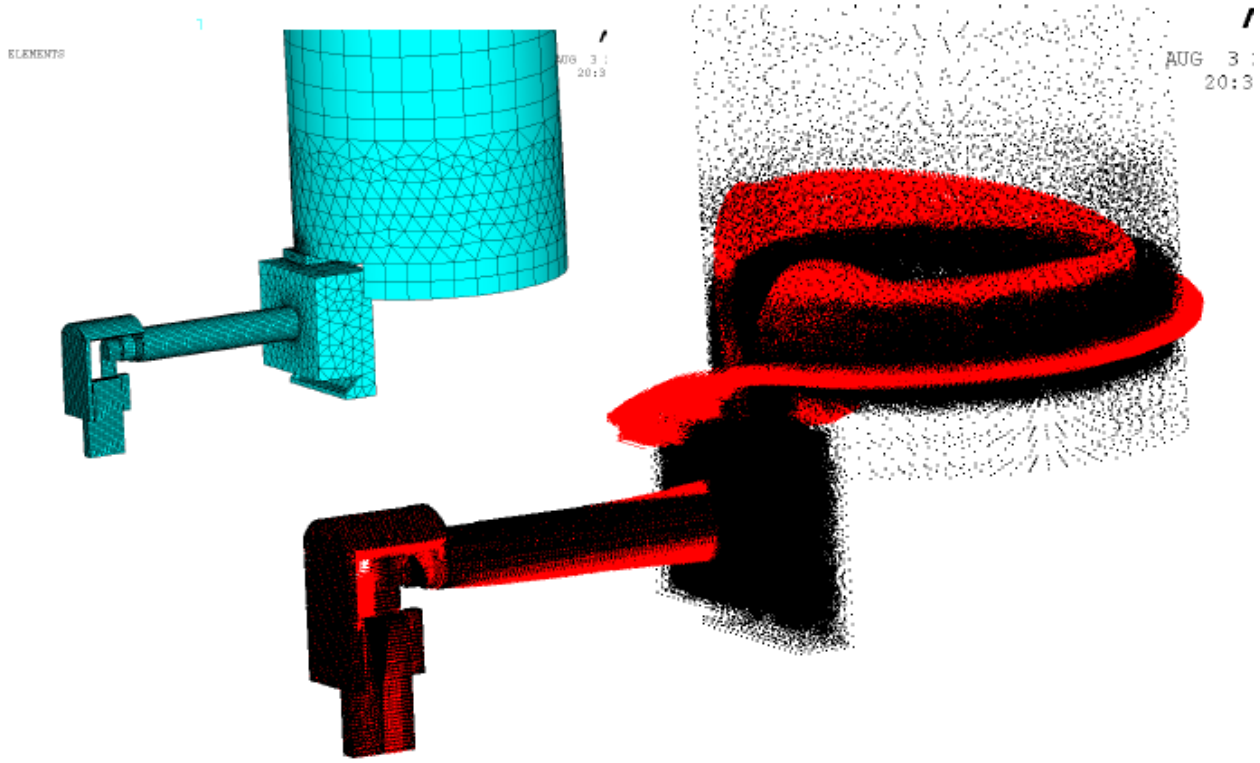

Nodal Lorentz Forces

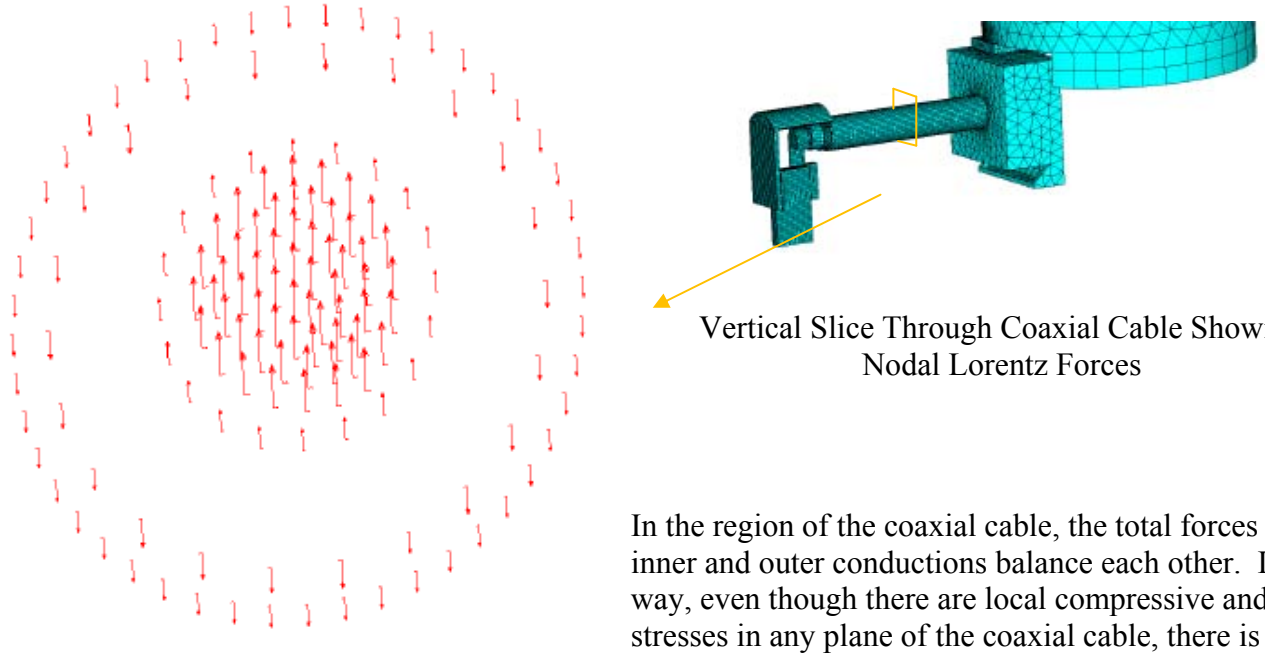

Vertical Slice Through Coaxial Cable Showing Nodal Lorentz Forces

In the region of the coaxial cable, the total forces on the inner and outer conductions balance each other. In this way, even though there are local compressive and tensile stresses in any plane of the coaxial cable, there is no net beam bending.

Lorentz forces on the embedded leads for Scenario 19 (instead of 13) were independently generated by Peter Titus using a different script, which can only operate on swept meshes of 8 node brick elements. The plots below compare the mechanical response for an artificially constrained mesh with nodal forces as computed by Titus and Mardenfeld, respectively, showing good agreement. Note that these stresses and deflections are not meaningful except as a measure of comparison.

	Titus' Fields	Fields Used in Stress Analysis
Mesh	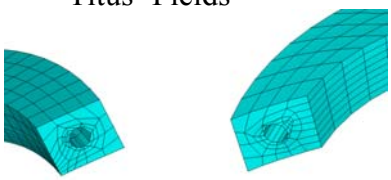	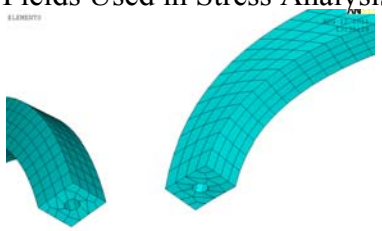
Boundary Conditions		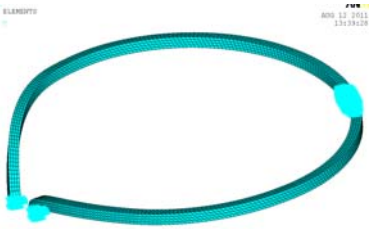
Nodal Lorentz Forces	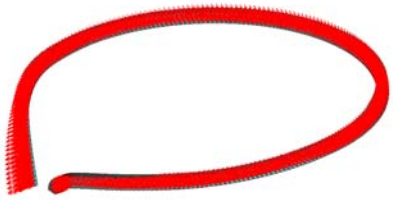	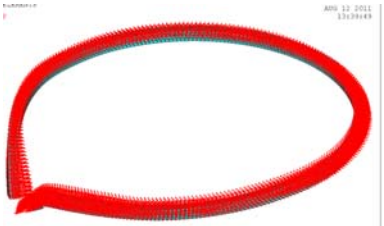
Displacement	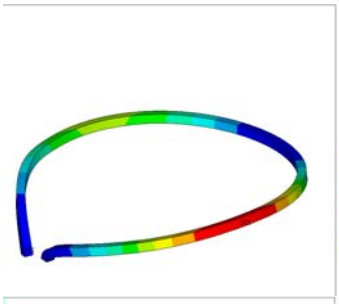	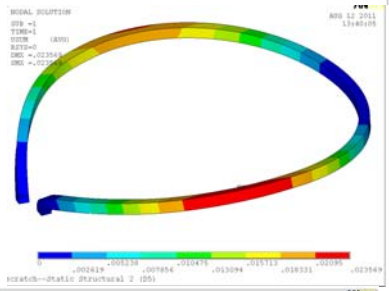
Stress Intensity	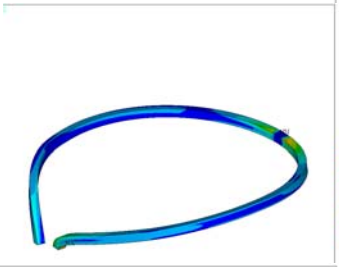	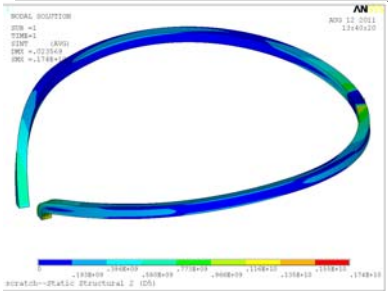
Stress Intensity Away from Boundary Conditions	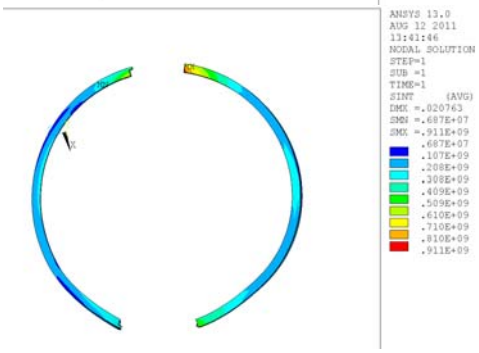	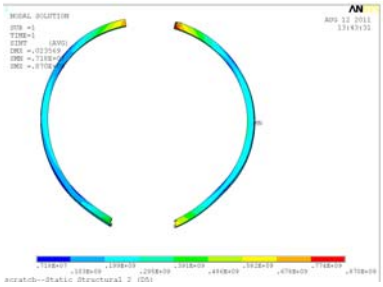

Stresses resulting from Lorentz forces only are shown below. Notice that the maximum deflection is less than 3/100 of a millimeter. Also, the peak stress intensity is approximately 12 Mpa at a corner which was modeled without a fillet. These values are low enough to be practically negligible.

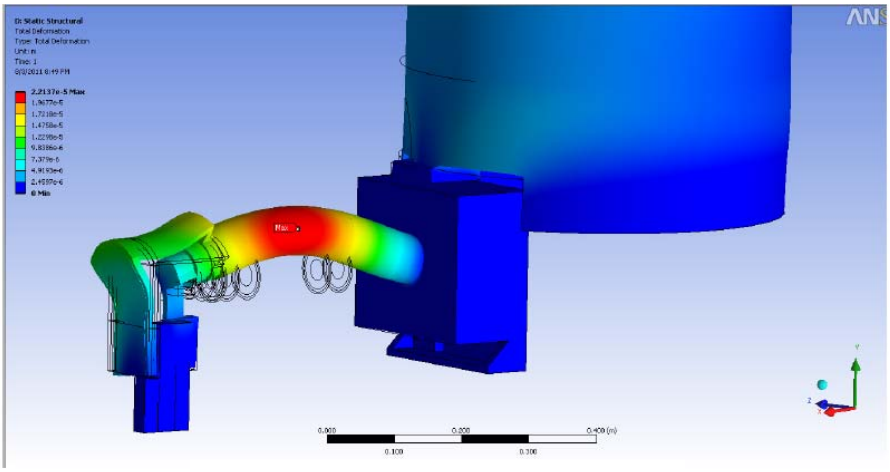

Deflection under Lorentz Loading

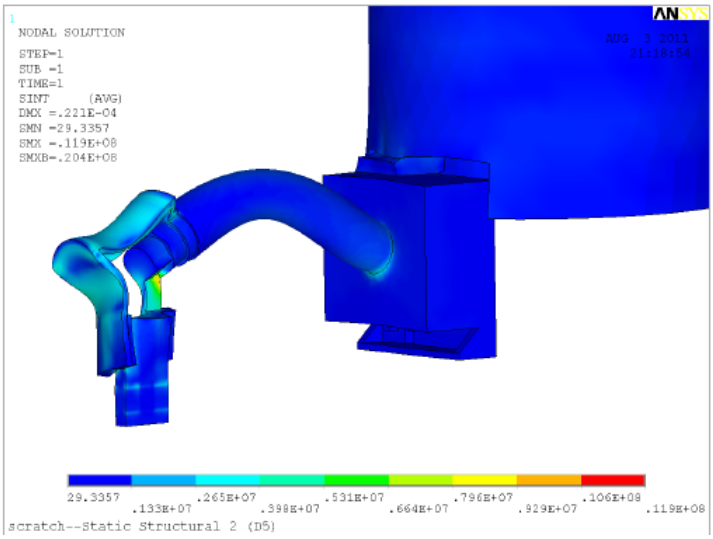

Stress Intensity under Lorentz Loading

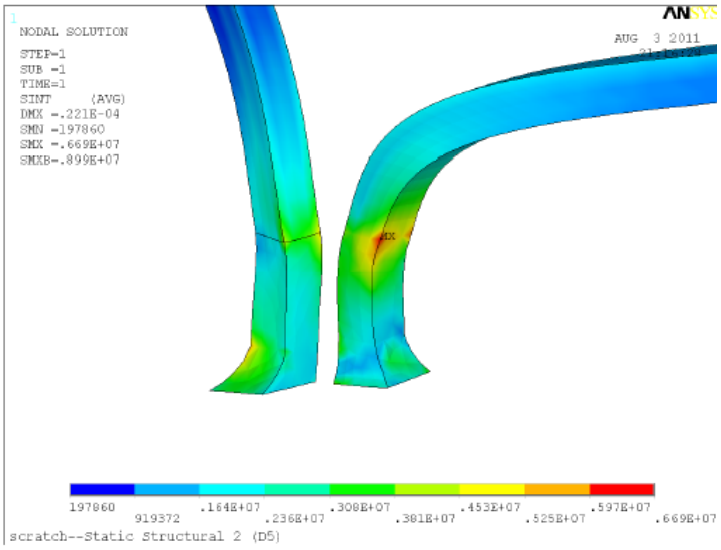

Deflection under Lorentz Loading Near Flag/Lead Interface

8.0 3d Model of Top of G10 Annulus

In the actual OH coil, the helical winding pattern creates complex, stepped three dimensional surfaces at the interface between the bottom of the coil proper and the top of the G10 support annulus. Prior modeling had assumed this as simple planar face, and computed shear stresses close to the fatigue allowable. Therefore, a second model was created with more accurate geometry in this region.

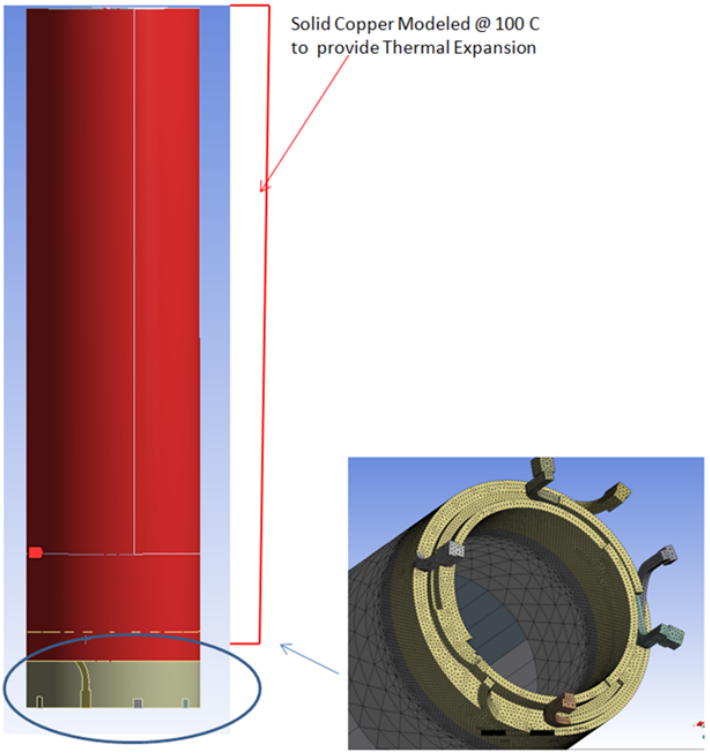

Complex Stepped Surfaces at Bottom of Coil

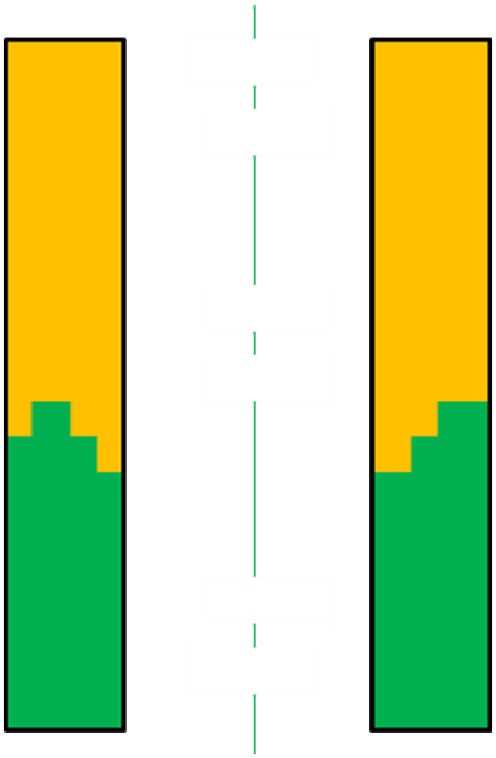

Schematic of OH Coil Section

The exact helical shape of the conductor was simplified into a series of steps, shown on the following page. The OH coil itself was modeled as pure copper, because the volume percent of turn to turn insulation is extremely small.

The entire OH coil and the electrical leads were assumed to be at uniform 100 C. The G10 annulus, and the copper water feeds (which have no current), were assumed to remain at room temperature. This represents the situation immediately after the pulse ends.

The bottom of the G10 annulus had fixed zero displacement, representing the bolted attachment to the steel pedestal. The top of the coil was left free to expand, in accordance with the compliance of the Belleville spring stack. The entire model used a continuous mesh, with no contact or nonlinearities.

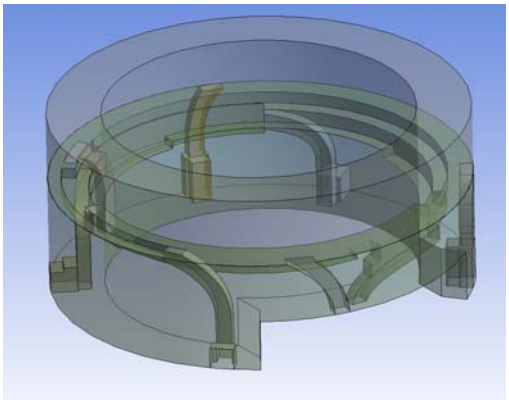

FEA Geometry

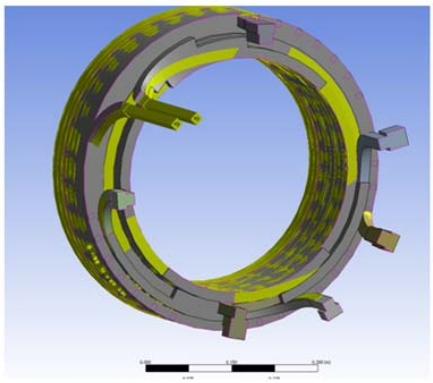

True Conductor Geometry, Yellow
overlaid on
FEA approximation

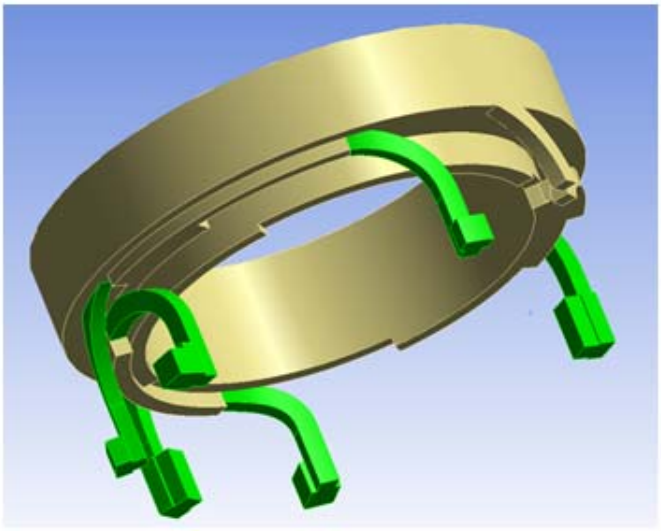

Water Feeds and G10 remain Cold

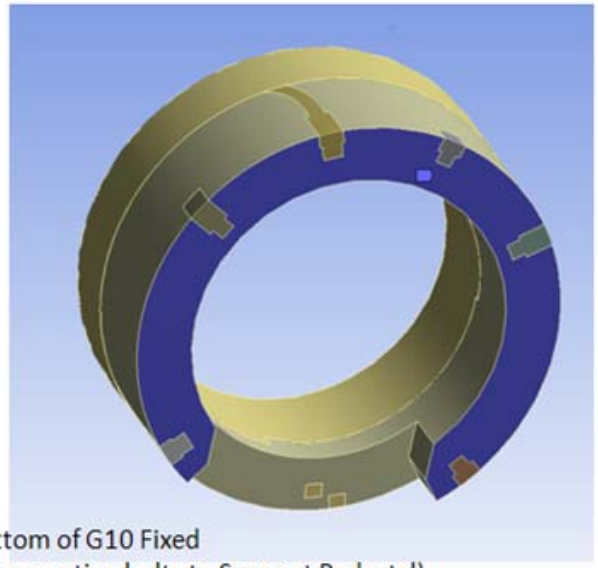

Bottom of G10 Fixed
(representing bolts to Support Pedestal)

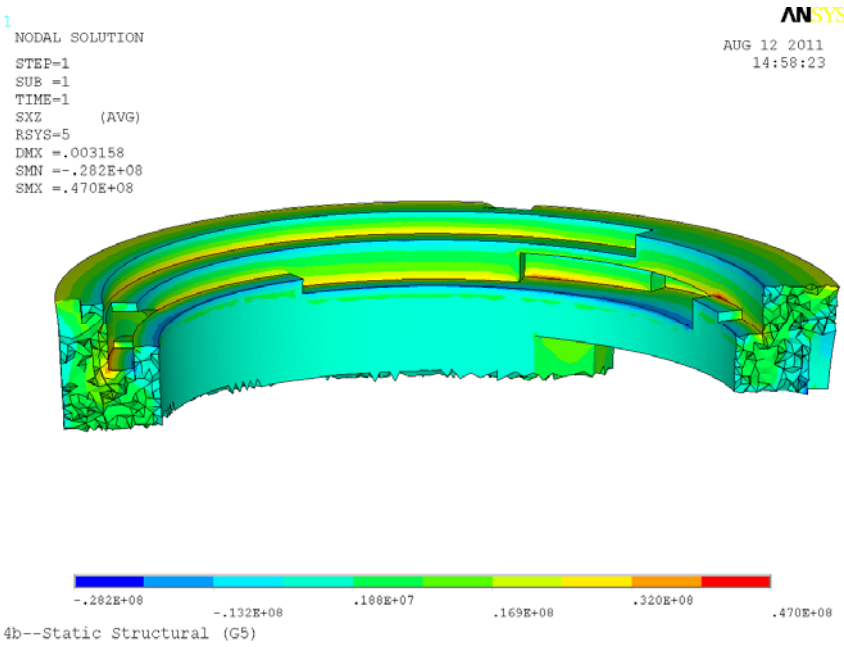

RZ Shear Stress, regions above the 5x Life fatigue allowable of 22 Mpa are Yellow, Orange, and Red

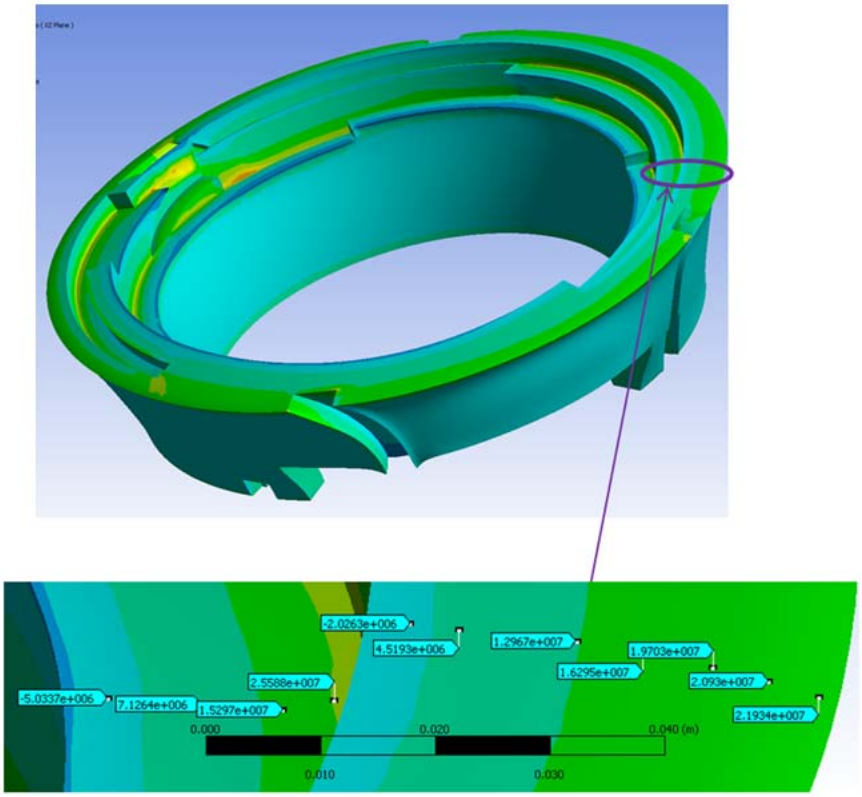

Close Up of RZ Shear Stress (Mpa)

These results verify that at the interface between the bottom of the OH coil and the top of the G10 annulus, shearing stresses are over 22 Mpa. Therefore it is imperative that for several turns near the very top and bottom of the OH coil, cyanate ester primer is applied during impregnation to increase adhesion strength.

Even with the added strength from the primer, eventual progressive delamination is possible, because locally the stresses exceed the 5x life S-N fatigue criteria, and the test specimens did not include Kapton insulation interleaved with the fiberglass cloth, which is present in the actual coil and has a tendency to reduce shear strength by a factor of ~ ½.

However, because these are thermally driven secondary stresses concentrated near the outer edges of the steps, because of the mechanical interlocking of the stepped surfaces and radial compression from the copper abutting against the G10 annulus ensuring gross structural stability, and because the Belleville washer stack at the top of the coil is designed to absorb any launching loads, this potential delamination is acceptable.

9.0 Analysis of Bus Bar Clamp and Lead Breakouts Before Recommended Changes

The three recommended design changes are: stiffening the support clamp between the top of the bus bar and the umbrella structure; includes a fillet at the joint between the lead flag and the conductor proper; and to implement active cooling on the bus bar. The third recommendation is justified by stress results in NSTXU-Calc-55-01-00, and by the transient thermal analysis (cool down), in Section 5.0. The other two are supported by the following analysis.

The interface between the top of the bus bar and the electrical jumpers to the coaxial cable is subject to a vertical load from thermal expansion of the bus bar, and a rotational torque from opposing vertical currents crossing the vertical and toroidal fields. Net reactions loads at a cut boundary slightly below this clamp were imported the finite element model documented in NSTXU-Calc-55-01-00, for scenario 72, shown in the figure below.

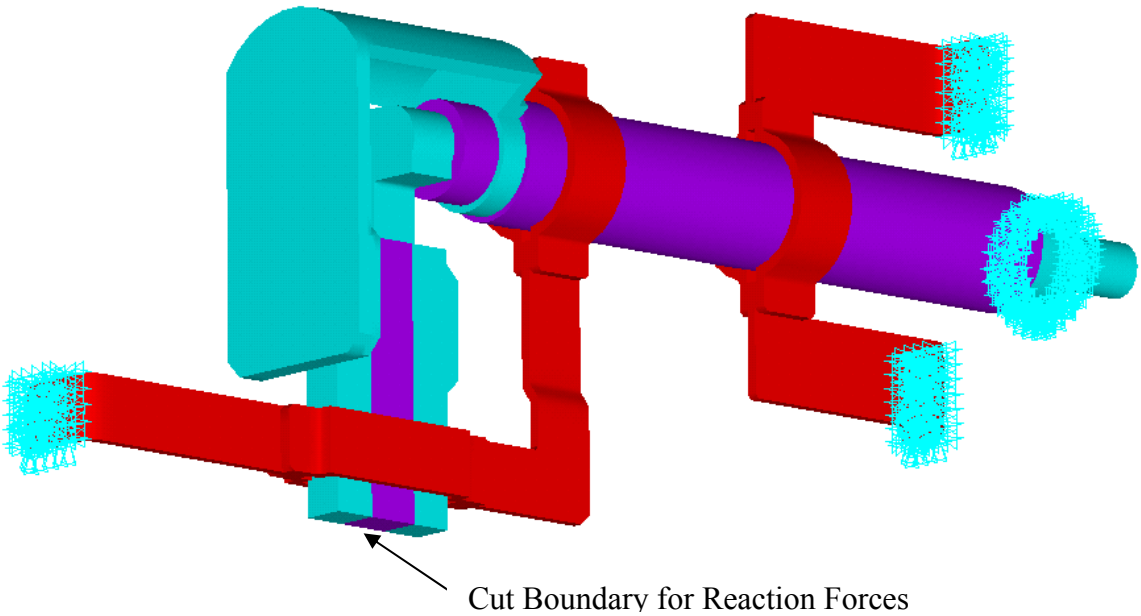

Cut Boundary for Reaction Forces

```
***** SUMMATION OF TOTAL    FORCES AND MOMENTS IN THE GLOBAL COORDINATE SYSTEM *****
 FX   =   -5797.393
 FY   =    603.8555
 FZ   =   -15229.90
 MX   =    71.33682
 MY   =   -11.79786
 MZ   =    49.08698
 HEAT=    290.5229
 AMPS=  0.4774847E-11
 FLUX=  0.4197038E-04

SUMMATION POINT= 0.79329      0.24829E-01 -2.6120
```

Nodal Forces Sum at Cut Boundary
Summation Point about Origin

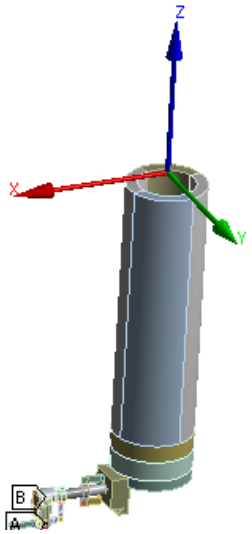

Coordinate System, Machine Horizontal Plane,
X Aligned with Centerline of Coaxial Cable

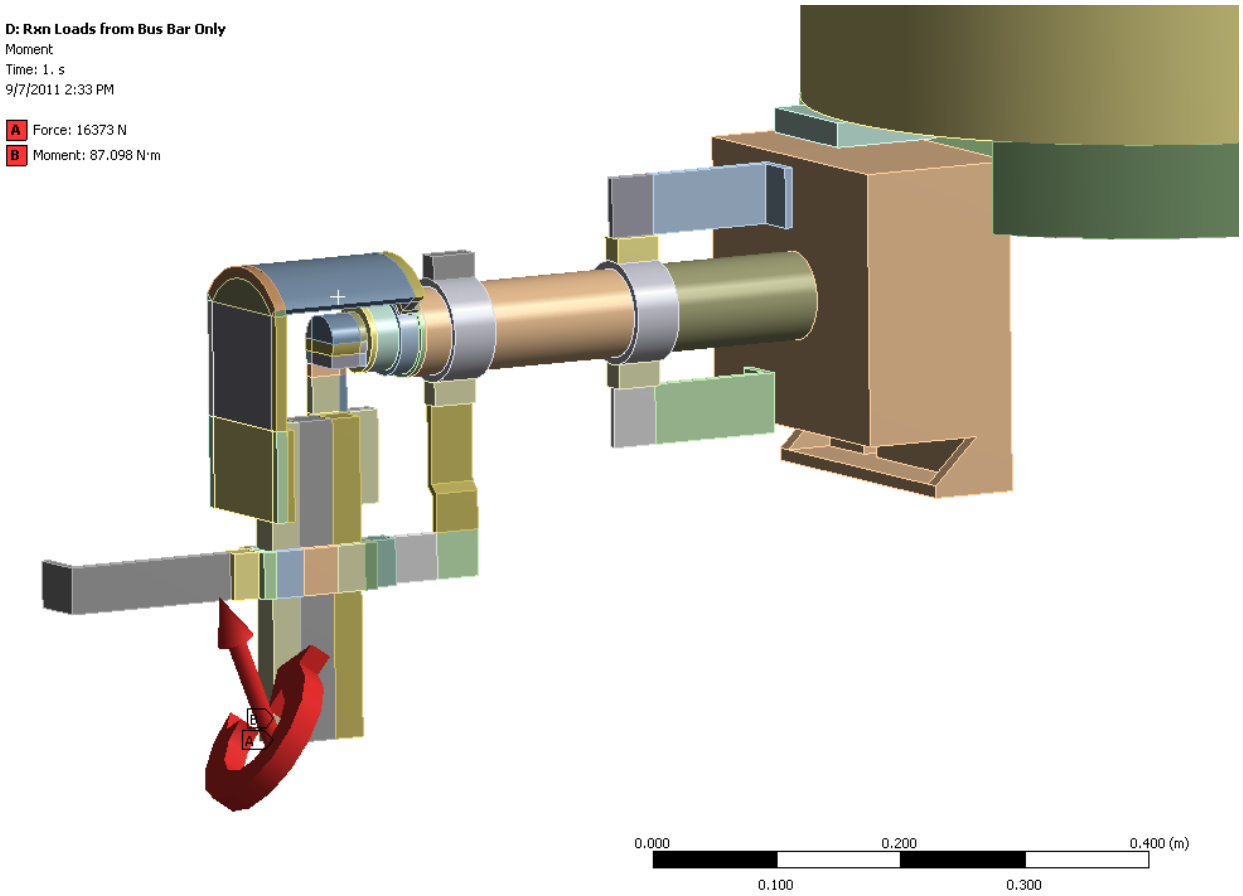

Reaction Loads Applied, Shown with Original Clamp Design

The figures on the following page show the resulting deflections and stresses from the bus bar reaction loads, without the thermal expansion or Lorentz loading on the rest of the bodies. The analysis was run with both the original clamp, and then with a stiffened alternative. This alternative clamp is not meant to be interpreted as a design suggestion, but rather to show the approximate size of a clamp required to structurally isolate the coaxial cable from the bus bar. This is an important distinction, because the interaction between the increased stiffness of the clamp and the strain controlled thermal expansion of the bus bar (which will be significantly less once active cooling is implemented) are not being considered. For this reason, the clamp will need to be revisited once the bus bar design is updated. However, the model is sufficient to show that the assumption from previous sections of a fixed boundary at the clamping surface can be achieved with a reasonably sized clamp, for example, square steel structural tubing, 7.5 cm side length, 1 cm wall thickness, and approximately 20 cm long.

For the original clamp design, stresses are unacceptably high, not only for the bus bar and clamp, but also for the coaxial cable components. Notice the stress intensity on the electrical jumper for the inner conductor of the coaxial cable is very close to the static allowable. The stiffer clamp reduces the stress in this location by a factor of 10, and the deflection by a factor of 100.

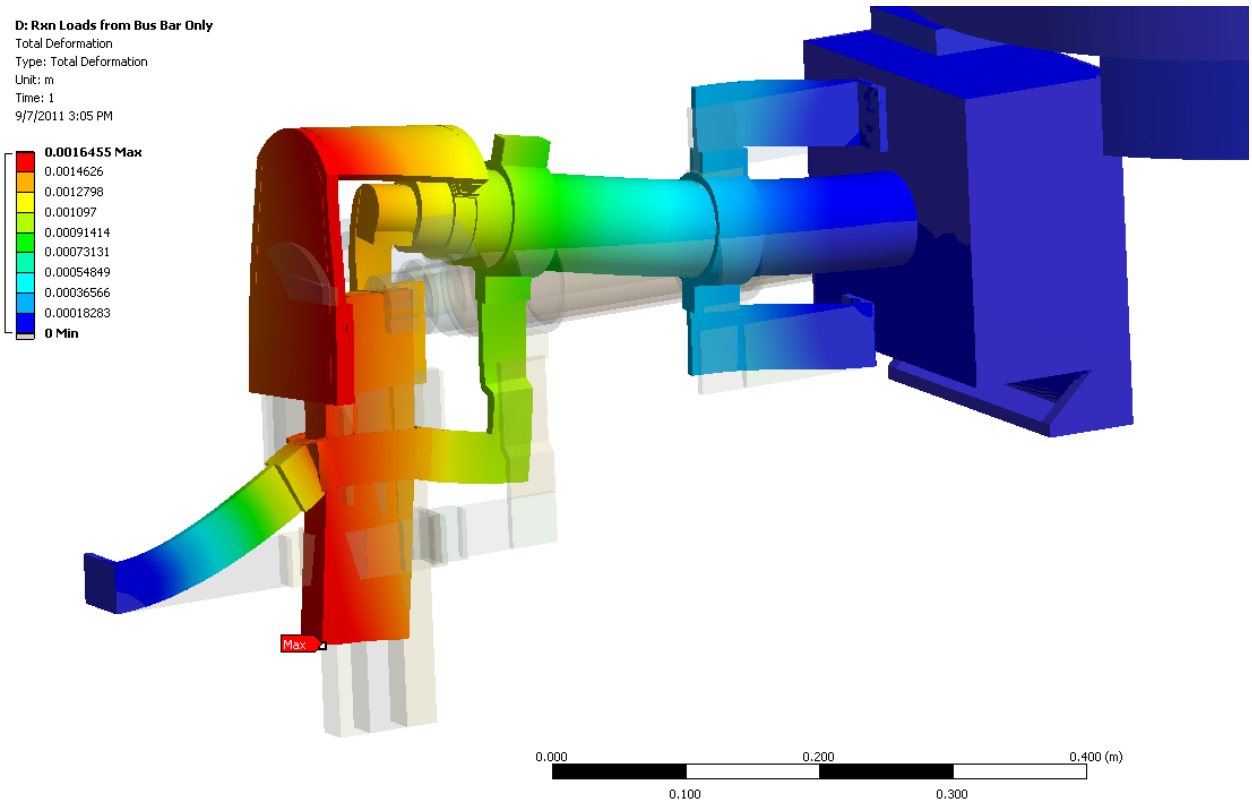
D: Rxn Loads from Bus Bar Only
Total Deformation
Type: Total Deformation
Unit: m
Time: 1
9/7/2011 3:05 PM
0.0016455 Max
0.0014626
0.0012798
0.001097
0.00091414
0.00073131
0.00054849
0.00036566
0.00018283
0 Min
Max
0.000
0.200
0.400 (m)
0.100
0.300

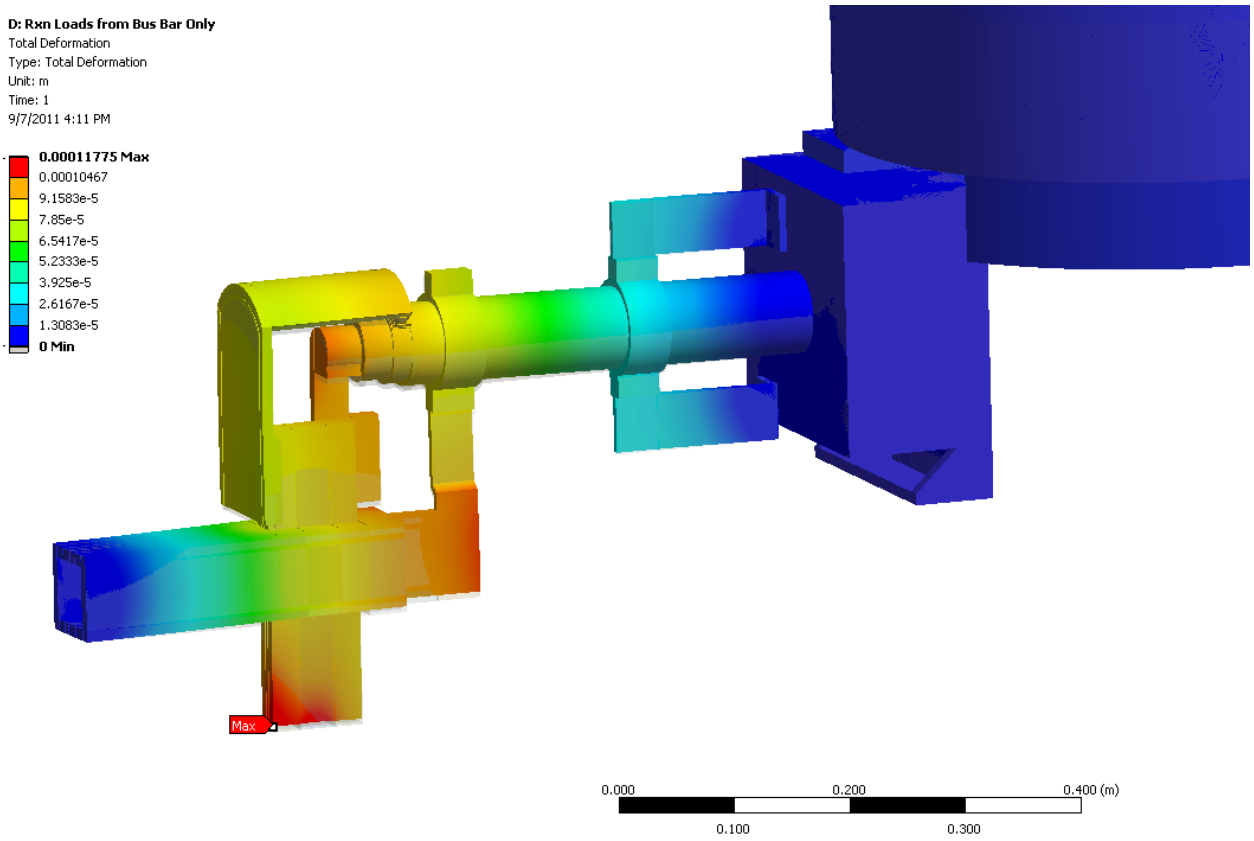
D: Rxn Loads from Bus Bar Only
Total Deformation
Type: Total Deformation
Unit: m
Time: 1
9/7/2011 4:11 PM
0.00011775 Max
0.00010467
9.1583e-5
7.85e-5
6.5417e-5
5.2333e-5
3.925e-5
2.6167e-5
1.3083e-5
0 Min
Max
0.000
0.200
0.400 (m)
0.100
0.300

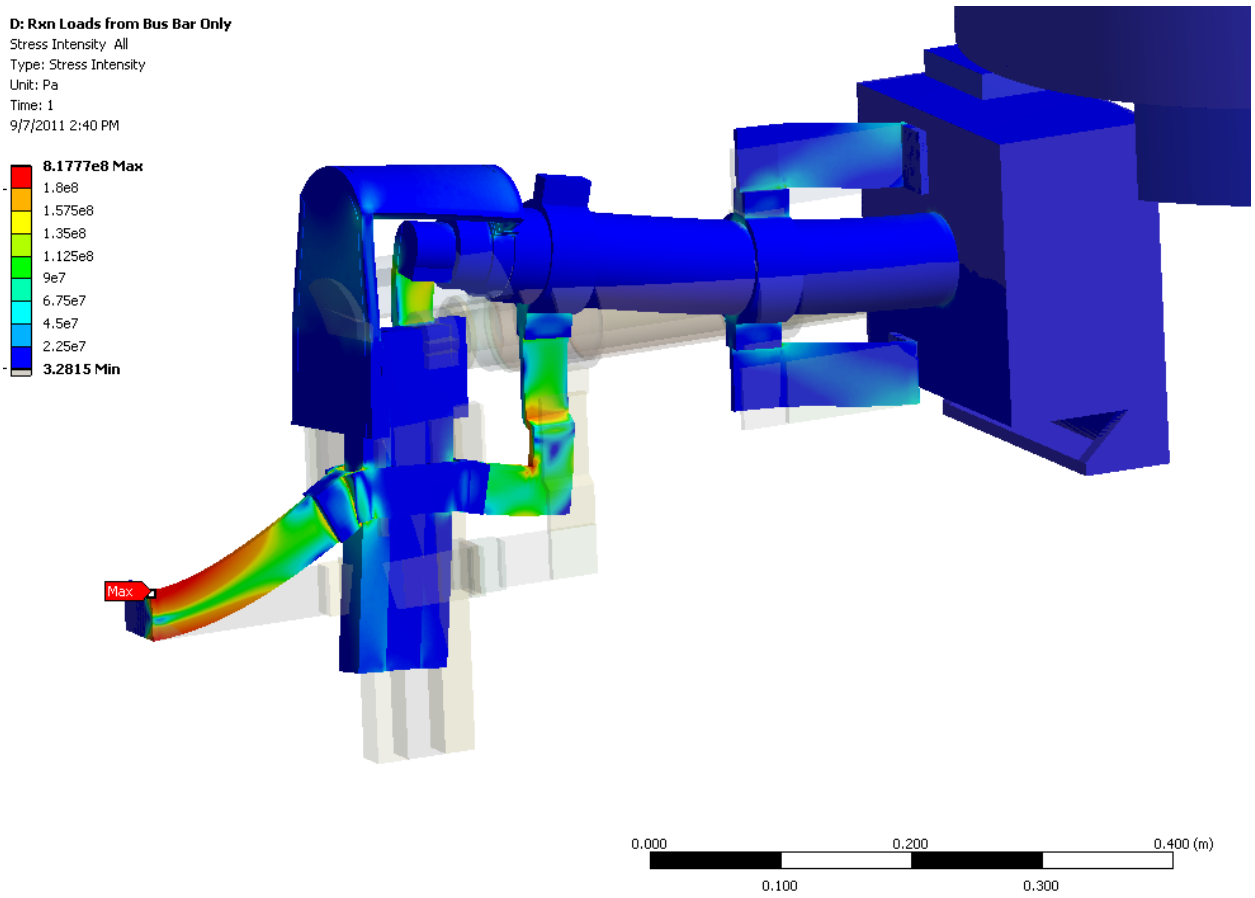
D: Rxn Loads from Bus Bar Only
Stress Intensity All
Type: Stress Intensity
Unit: Pa
Time: 1
9/7/2011 2:40 PM
8.1777e8 Max
1.8e8
1.575e8
1.35e8
1.125e8
9e7
6.75e7
4.5e7
2.25e7
3.2815 Min
Max
0.000
0.200
0.400 (m)
0.100
0.300

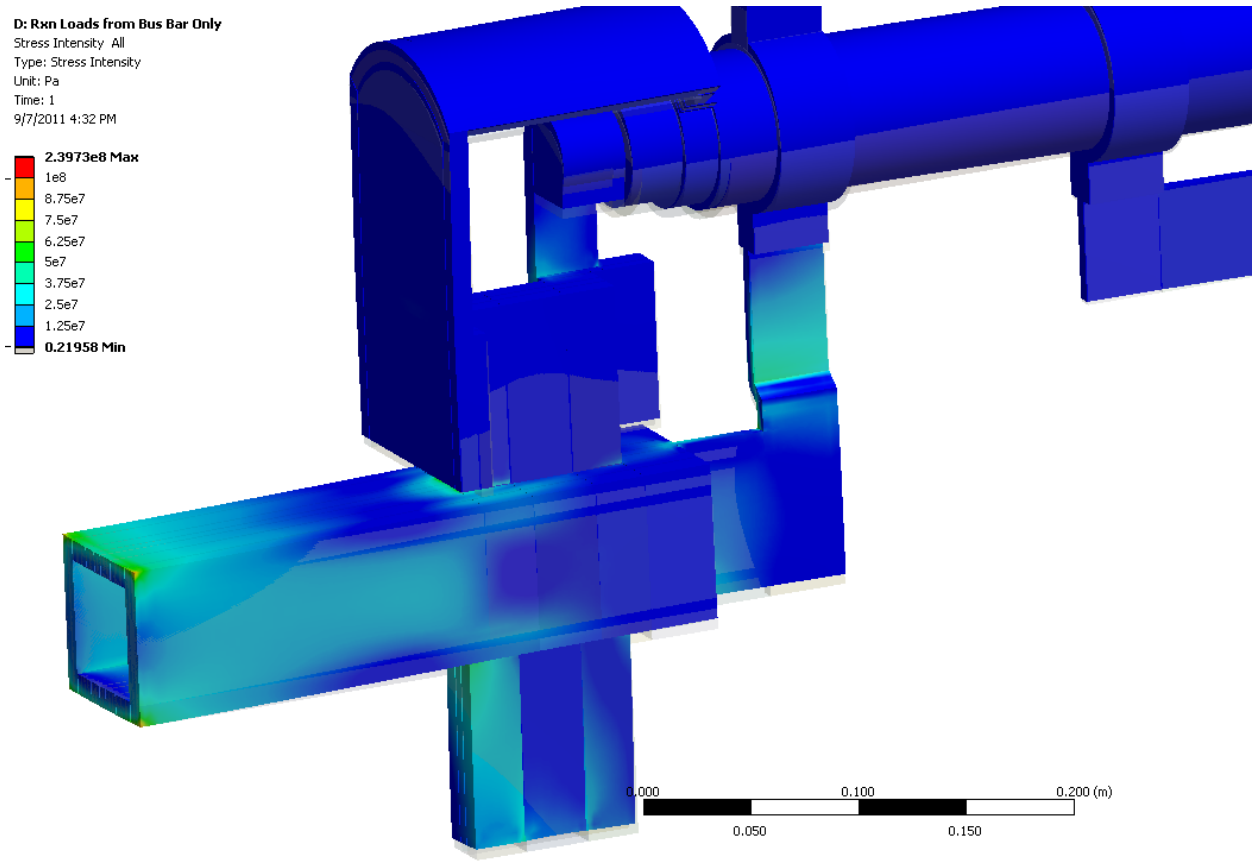
D: Rxn Loads from Bus Bar Only
Stress Intensity All
Type: Stress Intensity
Unit: Pa
Time: 1
9/7/2011 4:32 PM
2.3973e8 Max
1e8
8.75e7
7.5e7
6.25e7
5e7
3.75e7
2.5e7
1.25e7
0.21958 Min
0.000
0.100
0.200 (m)
0.050
0.150

The second recommend design change is at near the top of the flags, where they are brazed to conductor leads, shown below. There are several effects occurring in this region. First, there is a large gradient in the current density due to the abrupt change in area between the conductor and flags, creating a large thermal gradient near the braze. Second, the flags are held rigidly in place, while the coil expands radially outwards, imposing bending on the lead. Third, the vertically oriented currents leads are trapped between two vertically fixed surfaces, the bottom of the OH coil and the top of the lead flag, developing thermal stresses in the lead. Finally, in the original design a short segment of the lead was unembedded, compounding all of the previous problems at the structural discontinuities where the conductor "breaks out" of the G10 annulus, or "break in" to the flag at the weld.

The recommended design changes are to include a generous fillet near the top of the braze joint to smooth out the abrupt transition in cross section, and more importantly to make sure that the entire lead, all the way to the braze, is embedded in a structural filler material, such as a room temperature curing epoxy which can be field applied. This not only removes the structural discontinuities, but also changes the stress state so that it is primarily compressive, which greatly reduces the tendency for crack propagation.

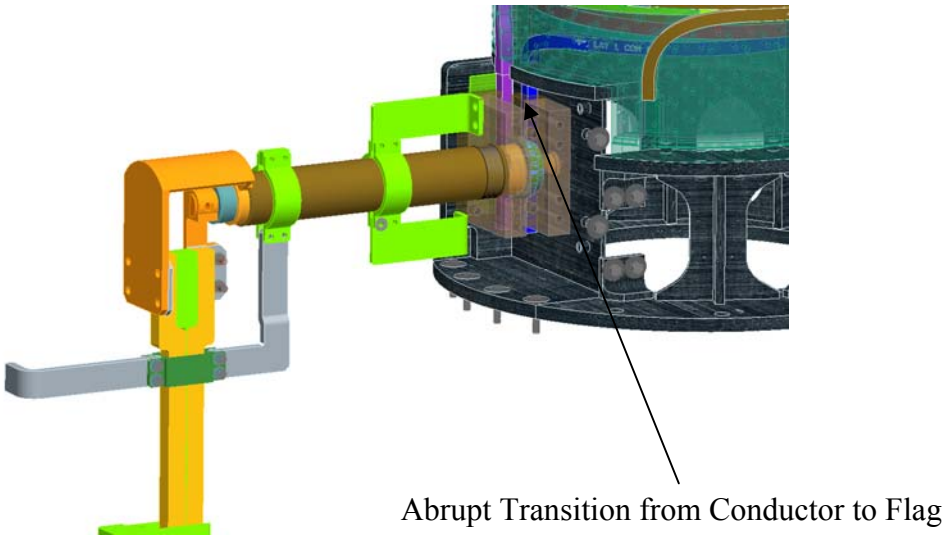

Inside the Coaxial Box

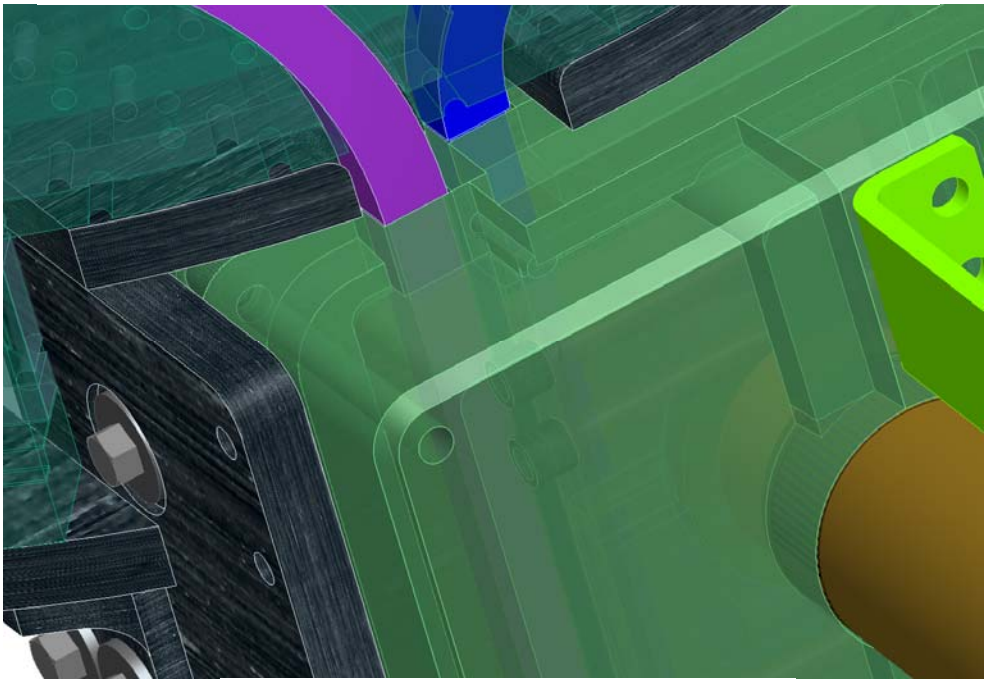

Close Up of Transition

This small region is not impregnated in the original design.
Recommend encapsulating entire lead, all the way up to the flag.

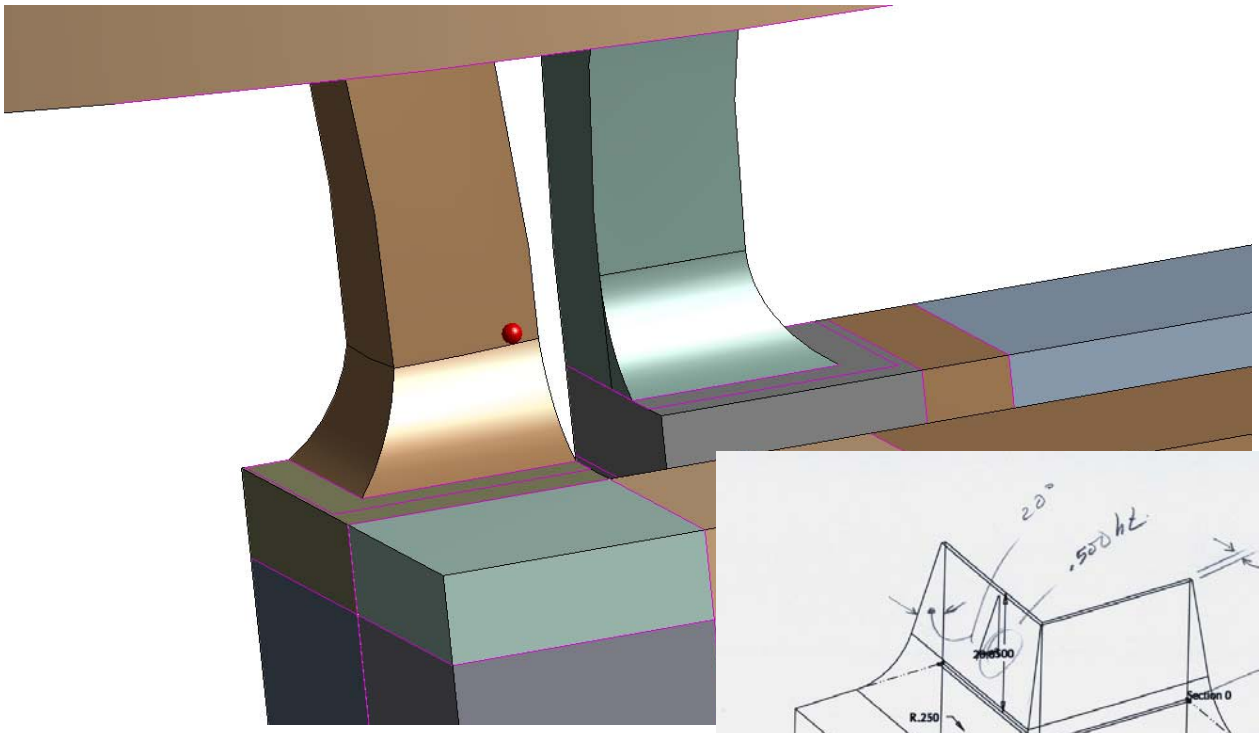

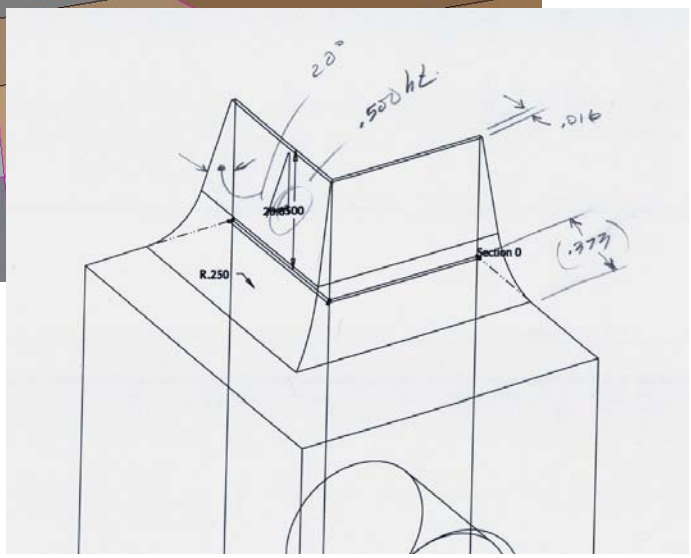

Recommend adding fillet to relieve stress concentrations at conductor/flag joint

The figure below shows the max principal stress without the fillets or encapsulation from thermal loads only. These values are as much as 3x higher than the fracture mechanics allowable of 125 Mpa. Although these are singularities, and the specific values may not be correct, the addition of an encapsulating material and fillets, results shown in section 5.0, actually turns these stresses almost entirely compressive locally, removing the facture initiation site in a region historically prone to cracking and water leaks.

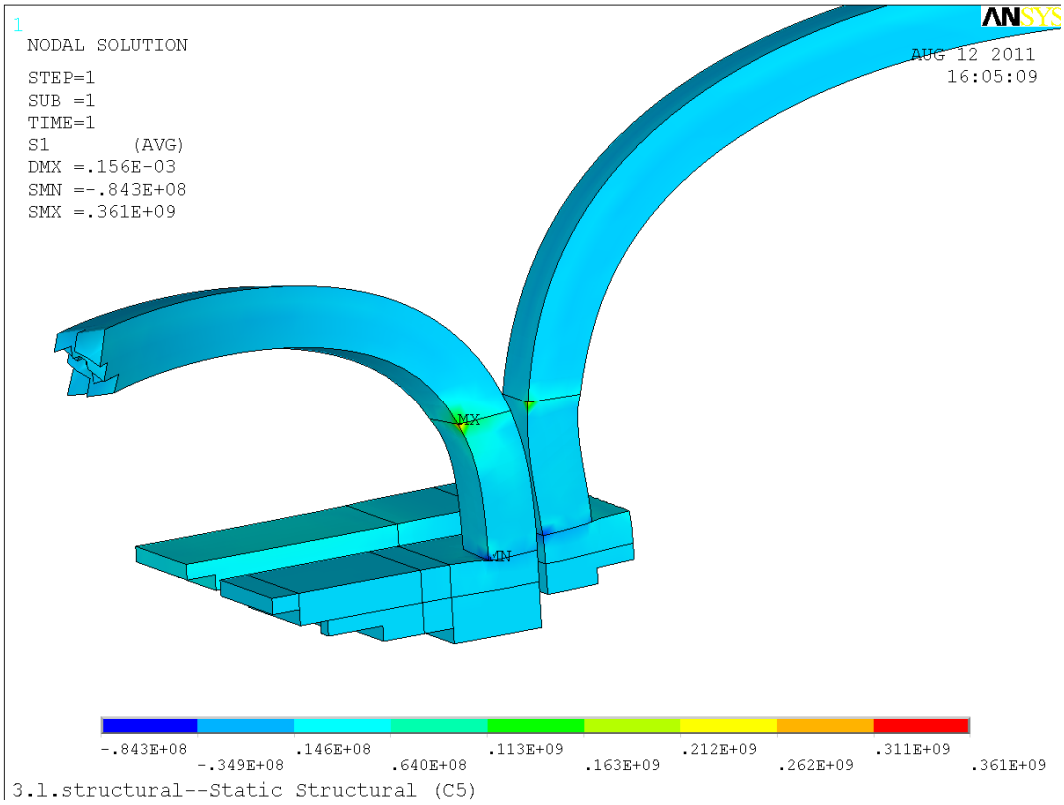

10.0 Conclusion

The purpose of this calculation is to qualify those components of the NSTX Upgrade which either provide an electrical path between the OH bus bar, and the body of the OH coil itself, or are ancillary structural members directly adjacent to this electrical path. Key Conclusions as are follows:

1. **The steel clamp connecting the bus bar to the skirt is not stiff enough as is, and will be need to be reinforced**. The stresses calculated with clamp as is are an order of magnitude too high. This is in agreement with the bus bar analysis (NSTXU-Calc-55-01). For this calculation, the clamp is assumed to be "infinitely rigid", by applying a fixed boundary at the bus bar/clamp interface. An appropriate clamp, which directs all bus bar reaction forces away from the coaxial cable, needs to be designed and qualified as acceptable for the bus bar.

2. **In the current design, there is a short section of conductor, where the leads "break out" of the G10 annulus and are brazed onto the lead flags, which is subject to particularly high thermal stress.** The lead flags should be slightly modified to include a fillet near this braze joint, and the conductor should be encapsulated with a structural filler material (i.e. glass reinforced room temperature curing epoxy). With these modifications, the peak tensile principle stress is reduced to ~ 80 Mpa, and the peak Stress Intensity is reduced to ~ 190 Mpa, which are within allowable.

3. **Per results of NSTXU-Calc-55-01, the OH bus bars will be modified to include active cooling.** The inlet temperature for this coolant should be the same as the inlet temperature for the OH coolant water, nominally 12 C. Furthermore, the coolant inlet should be near the coaxial cable end of the bus bar, and the outlet should be at the power supply side of the bus bar, such that the water is flowing away from the machine. In this way, thermal gradients across the coaxial cable are minimized, and there is sufficient conduction from the coaxial cable to the actively cooled bus bar and lead flags that there will be no ratcheting, and the coax will cool down completely between shots.

4. **Provided adequate structural support redirects bus bar reaction forces away from the coax per item one, Lorentz forces are not high enough to be of any significance. These components are overwhelmingly driven by thermal effects.** During normal operation, local peak stress intensity and tensile principal stresses from electromagnetic forces only are ~ 25 Mpa and 7 Mpa respectively, with membrane stresses << 10 Mpa. Although only electromagnetic equilibria were considered, these values are so low that even if they were doubled during transients or disruptions, the stresses would still be acceptable.

5. **The delaminating shearing stresses on the lead are of order 60 Mpa, above the fatigue allowable**. In the region, local delamination is expected, and acceptable, because testing has shown that it occurs in a predictably benign fashion, and the G10 Annulus will provide sufficient structural stability and dielectric strength.

6. **The shearing stress between the G10 Annulus and the lower most turns of the OH coil is of order 20 Mpa.** This is caused by the interaction between radial thermal expansion of the OH coil, and the fixity of the bottom of the cold G10 Annulus. The conductor within several layers of either the top or bottom of the OH coil should be sandblasted and primed to locally increase the shear strength. Locally these stresses are still above the 5x life fatigue requirement, after applying a 50% knockdown factor for interleaved Kapton. Progressive local delamination is likely, but judged acceptable.

Provided the recommended design changes are addressed, the analysis concludes that the thermal and mechanical response of OH coaxial and embedded leads are within acceptable ranges.